The Astrophysical Journal, 719:240–263, 2010 August 10 doi:10.1088/0004-637X/719/1/240

THE LICK/SDSS LIBRARY. I. SYNTHETIC INDEX DEFINITION AND CALIBRATION

M. Franchini[1], C. Morossi[1], P. Di Marcantonio[1], M. L. Malagnini[2], and M. Chavez[3]
[1] INAF—Osservatorio Astronomico di Trieste, Via G.B. Tiepolo, 11, I–34131 Trieste, Italy; franchini@oats.inaf.it, morossi@oats.inaf.it, dimarcan@oats.inaf.it
[2] Dipartimento di Fisica–Sezione di Astronomia, Università degli Studi di Trieste, and INAF, Via G.B. Tiepolo, 11, I–34131 Trieste, Italy; malagnini@oats.inaf.it
[3] Instituto Nacional de Astrofísica, Optica y Electrónica, Luis Enrique Erro 1, 72840, Tonantzintla, Puebla, Mexico; mchavez@inaoep.mx
Received 2010 September 3; accepted 2010 June 13; published 2010 July 19

ABSTRACT

A new synthetic library of spectral feature indices, Lick/Sloan Digital Sky Survey (SDSS), for stellar population studies is presented. Lick/SDSS is computed from synthetic spectra with resolving power $R = 1800$ to fully exploit the content of the spectroscopic SDSS–DR7 stellar database. The Lick/SDSS system is based on the Lick/IDS one complemented with a UV index in the wavelength region of Ca II H and K lines. The system is well suited to study α-element abundances in F, G, and K stars. The reliability of synthetic indices in reproducing the behaviors of observational ones with effective temperature, surface gravity, overall metallicity, and α-element abundances is tested by using empirical stellar libraries (ELODIE, INDO–U.S., and MILES) and the SDSS–DR7 spectroscopic database. The importance of using the same temperature scale in comparing theoretical and observational indices is discussed. The full consistency between Lick/SDSS and observational indices derived from the above mentioned stellar libraries is assessed. The comparison with indices computed from SDSS–DR7 spectra evidences good consistency for "dwarf" stars and significant disagreement for "giant" stars due to systematic overestimation of the stellar $T_{\rm eff}$ by the SEGUE Stellar Parameter Pipeline.

Key words: galaxies: stellar content – stars: fundamental parameters – stars: late-type

Online-only material: color figures

1. INTRODUCTION

The study of stellar populations is a fundamental tool for the understanding of the physical processes involved in the formation and evolution of galaxies. Of particular interest, as building blocks of a stellar population, is the analysis of F, G, and K stars which, due to their long lifetimes, provide information on the environment chemical composition at different star formation episodes. In fact, the study of abundance patterns like, for example, α-element enhancement, gives insight into the role of SNe I and SNe II in the chemical enrichment of galaxies. Out of the many papers (e.g., Vazdekis 1999; Bruzual & Charlot 2003; Le Borgne et al. 2004; Maraston 2005; Trager et al. 2008) in the literature for studying this topic in single stellar populations, several authors (e.g., Schiavon 2007; Lee et al. 2009) used an approach based on the analysis of integrated Lick/IDS indices (WFGB94; Worthey et al. 1994). Unfortunately, the Lick/IDS system was defined at a resolution that is much lower than those of the databases available from recent and forthcoming surveys like, for example, the Sloan Digital Sky Survey (SDSS; York et al. 2000) and the Large Sky Area Multi-Object Fiber Spectroscopic Telescope survey (LAMOST; http://www.lamost.org/). Furthermore, as discussed in WFGB94, several uncertainties in both IDS response function and wavelength calibration make it difficult to transform new observational indices into the original Lick/IDS system thus introducing possible systematic errors.

It must also be recalled that the use of empirical libraries in stellar population studies requires an extrapolation to abundance patterns that differ from those of the library stars, which are mostly from local systems (in general from the solar neighborhood). Therefore, models based on empirical libraries cannot easily reproduce the integrated spectra of systems whose star formation histories are different from those of local systems. It is therefore mandatory to complement empirical libraries with theoretical ones even if it is a difficult task to compute reliable high-resolution synthetic spectra in an extended stellar parameter space and in a wide spectral region. In fact, such a computation requires an extensive and reliable list of atomic and molecular line opacities. Moreover, exhaustive checks on how well the synthetic quantities match the observations of real stars must be passed before safe use of any synthetic library.

Along this line, several authors already published synthetic libraries of Lick/IDS indices in order to complement the observed ones to synthetize spectral energy distributions (SEDs) of a stellar population (Tripicco & Bell 1995; Korn et al. 2005; Coelho et al. 2005).

In this work, which is the first of a series, we present a new synthetic library (hereafter Lick/SDSS) of indices in a Lick-like system fine-tuned to analyze data at SDSS and LAMOST resolution. The Lick/SDSS library is aimed at applications in stellar population synthesis, specifically to the study of old and intermediate-age stellar populations and provides a useful tool for F, G, and K stellar atmospheric parameter determinations[4] (examples of this kind of application can be found in Cayrel et al. 1991; Franchini et al. 2004; Willemsen et al. 2005; Girard & Soubiran 2005; Valenti & Fischer 2005).

The Lick/SDSS indices are derived from a new set of absolute flux-calibrated synthetic spectra computed in the temperature range of F, G, and K stars assuming solar-scaled and α-enhanced chemical mixtures. The synthetic spectra are aimed at applications in stellar population synthesis and can be used to get element-by-element abundances at medium spectral resolution in Galactic stars and extragalactic stellar populations. In particular, we plan to use them to analyze the thousands of spectra which will be provided by the forthcoming Medium Resolution Spectroscopic Survey with LAMOST (Zhao et al. 2006). On the other hand, the direct use of them to study

[4] In the second paper of this series we will use the Lick/SDSS library for deriving new estimates of atmospheric parameters and, in particular of [Ca/Fe] and [Mg/Fe], of SSDS–DR7 (Abazajian et al. 2009) stars.

low-resolution and low signal-to-noise ratio (S/N) spectra like the SDSS–DR7 ones is less straightforward so that it is more convenient, in such a case, to adopt a "spectral feature index" approach. Therefore, we degrade our synthetic spectra to $R = 1800$ in order to match the resolution of SDSS–DR7 (Abazajian et al. 2009) spectra and compute synthetic Lick/SDSS indices by using the same nominal Lick/IDS wavelength band definitions of WFGB94. Moreover, due to the still good quality of SDSS–DR7 spectra in the region of Ca II H and K, we extend the index list by introducing a new index, CaHK, which increases the sensitivity of our system to calcium abundance. It is worthwhile noticing that the use of $R = 1800$ instead of $R\sim630$ (Lick/IDS resolution) allowed us to avoid any loss of information that could occur in degrading SDSS–DR7 spectra to the resolution of IDS spectra.

This paper is organized as follows: in Section 2, we describe the computation of the synthetic spectra, the production of the synthetic Lick/SDSS indices and their calibration; Section 3 presents the success of a validity check on the accuracy of Lick/SDSS in reproducing observational indices of solar neighborhood stars; Section 4 describes the comparison of Lick/SDSS prediction with empirical indices computed from SDSS–DR7 spectra of F, G, and K stars. A summary is given in Section 5.

2. THE SYNTHETIC INDICES

2.1. Synthetic Spectra and Atmosphere Models

A comprehensive set of 2550 synthetic spectra has been computed at wavelength sampling $\Delta\lambda = 0.05$ Å, rotational velocity of 0 km s^{-1}, and microturbulent velocity $\xi = 2$ km s^{-1} in the wavelength range 3000–7000 Å. The spectra were computed by means of the stellar spectral synthesis program SPECTRUM v2.75[5] (Gray & Corbally 1994) using the cool4.iso.lst line list kindly provided to us by R. O. Gray (2009, private communication). SPECTRUM computes the LTE synthetic spectrum given a stellar atmosphere model. For our purposes, the models from the "New Grids of ATLAS9 Model Atmospheres" by Castelli & Kurucz (2003) and F. Castelli (2003, private communication), computed with updated Opacity Distribution Functions (hereafter newODFs), were adopted in the following ranges of atmospheric parameters.

1. Effective temperature from 3500 to 7000 K at a step of 250 K.
2. Surface gravity from 0.5 to 5.0 dex at a step of 0.5 dex.

Two different assumptions on chemical composition lead to two different grids of models and synthetic spectra. The first one (SSA grid) refers to Solar Scaled Abundances (based on Grevesse & Sauval 1998) at overall metallicities [M/H] = −2.5, −2.0, −1.5, −1.0, −0.5, 0.0, 0.2, 0.5 (Z = 0.00006, 0.0002, 0.0005, 0.002, 0.005, 0.017, 0.026, 0.051). The second one (NSSA grid) refers to Non-Solar Scaled Abundances with enhanced α over iron ratios [α/Fe] =+0.4, and [Fe/H] =−4.0, −2.5, −2.0, −1.5, −1.0, −0.5, 0.0, 0.2, 0.5 (Z = 0.000004, 0.0001, 0.0004, 0.001, 0.004, 0.011, 0.034, 0.052, 0.097). The α elements considered are O, Ne, Mg, Si, S, Ar, Ca, and Ti, and both SSA and NSSA include molecular opacities from H_2, CH, NH, OH, MgH, SiH, CaH, C_2, CN, CO, SiO, and TiO.

Particular attention was taken to have full consistency between the computed synthetic spectra and the newODFs of the atmosphere models. Therefore, even if the use of a fixed value for ξ is somewhat arbitrary (see Kurucz 1996 for a detailed discussion), $\xi = 2$ km s^{-1} was imposed by the characteristics of the newODFs.

2.2. Index Measurement

Out of the 25 Lick/IDS indices given in Table 1 of Worthey et al. (1994), 19 indices were measured on our synthetic spectra by using the most up-to-date band definitions from http://astro.wsu.edu/worthey.[6] An additional index that we call CaHK was introduced to describe the behavior of calcium H and K lines by using a central passband in the wavelength range 3900 Å–4000 Å and the two pseudo-continuum passbands 3837 Å–3877 Å and 4040 Å–4080 Å. This index differs from that one defined by Serven et al. (2005; aside from the definition of the pseudo-continuum blue band that we moved to longer wavelengths to avoid the low S/N of the bluest part of SDSS spectra) because the wavelength regions of the line cores ($\lambda_c \pm 2.5$ Å) were removed from the central bandpass to avoid regions that can be affected by chromospheric emission in the observed spectra of cool stars.[7] We express broad features measuring molecular bands such as CN_1, CN_2, Mg_1, and Mg_2, as usually, in magnitudes, while narrow features primarily due to atomic species are expressed in Å.

Since we want to use our synthetic indices to analyze SDSS spectra each synthetic spectrum was degraded to the SDSS resolution ($R = 1800$, FWHM = 166 km s^{-1}) before the actual computation of the indices.[8]

2.3. α-element Dependency

The effects of α-element enhancement on the 20 indices is investigated by comparing the predictions of the NSSA grid with those from the subset of the SSA grid with the same [Fe/H] values. We remind the reader that for the SSA grid [Fe/H] and [M/H] coincide while this is not true for the NSSA grid. The direct comparison of NSSA and SSA individual indices at the same ($T_{\rm eff}$, log g, [Fe/H]) values is shown in Figure 1. For comparison purposes let us divide the description of the indices into two temperature intervals. For $T_{\rm eff} \geqslant 4250$ K (indicated with blue dots in Figure 1) we can cluster the indices into three groups:

1. *The* [α/Fe] *sensitive group*. This group contains eight indices, namely, CaHK, CN_1, CN_2, Ca4227, Fe4668, Mg_1, Mg_2, and Mgb. In all the cases but Mg_1 the NSSA index values are larger (CaHK, Ca4227, Mg_2, and Mgb) or smaller (CN_1, CN_2, and Fe4668) than the corresponding SSA ones. In general, the differences vanish with the vanishing of the indices themselves, i.e., at high temperatures. It is worthwhile to notice the odd negative values of SSA CaHK for intermediate temperatures (4500–6000 K) and non-supergiant surface gravities. These negative values are

[5] http://www1.appstate.edu/dept/physics/spectrum/spectrum.html

[6] The other six indices in the Lick/IDS system, namely, TiO_1 and TiO_2, and the Hγ and Hδ pairs (Worthey & Ottaviani 1997) were not computed because they are relevant only outside the effective temperature range considered in this paper.

[7] An estimate of the effect of Wilson–Bappu CaHK fill-in can be obtained by comparing CaHK index values for two stars (HD 237903 and G 19-24) with almost equal photospheric spectra in the 3800 Å–4100 Å region but different chromospheric emissions. The removal of the line cores in the CaHK index computation reduces the difference in the index values of the two stars from 9% to 2%, i.e., below observational uncertainties (see Table 1).

[8] This resolution is also close to that of LAMOST low-resolution half slit width, thus making it possible to use the same synthetic indices also in the LEGUE (Newberg et al. 2009) framework.

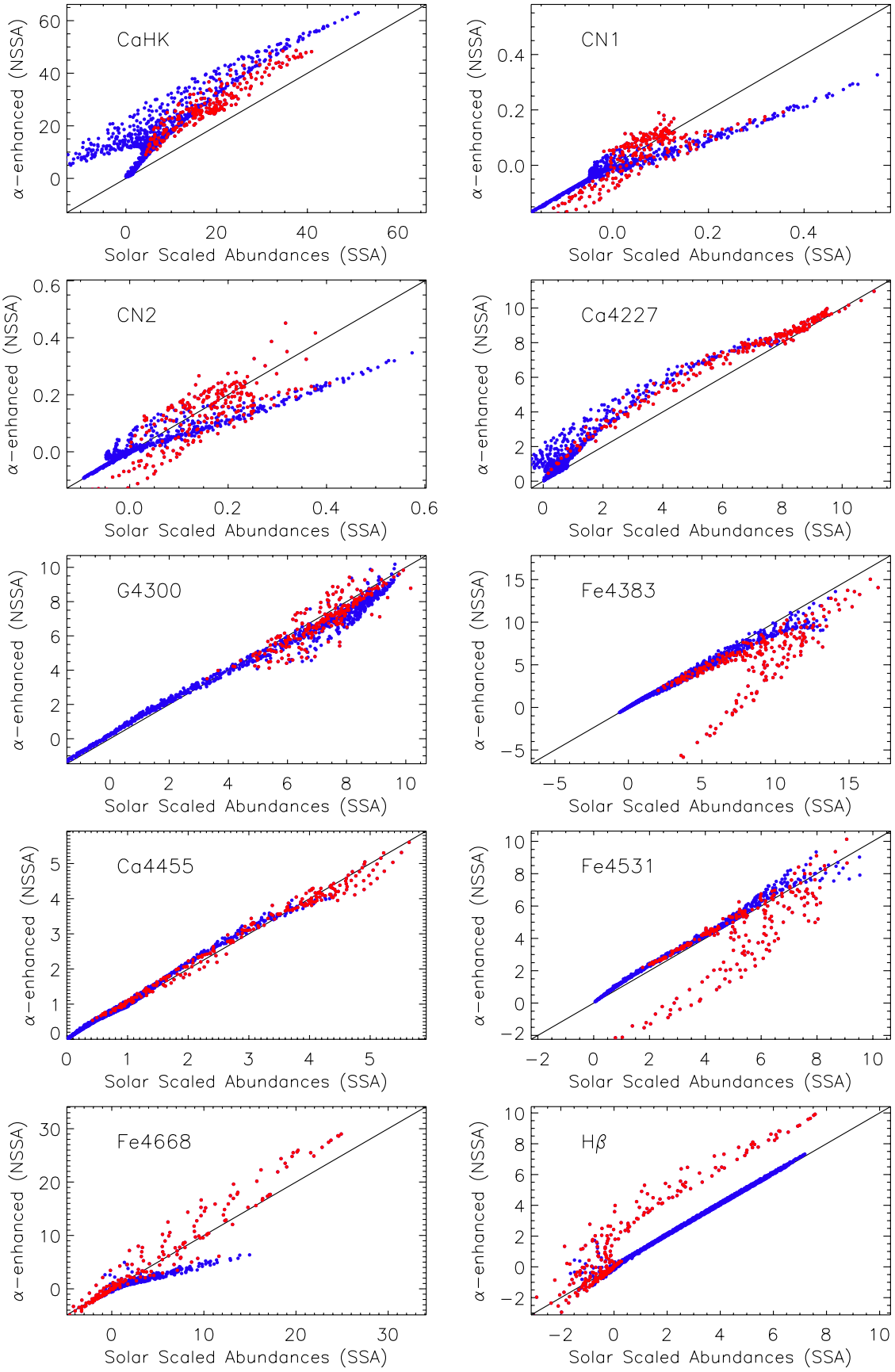

Figure 1. Spectral index response to [α/Fe]: $T_{\rm eff} \geqslant 4250$ blue points; $T_{\rm eff} < 4250$ red points.
(A color version of this figure is available in the online journal.)

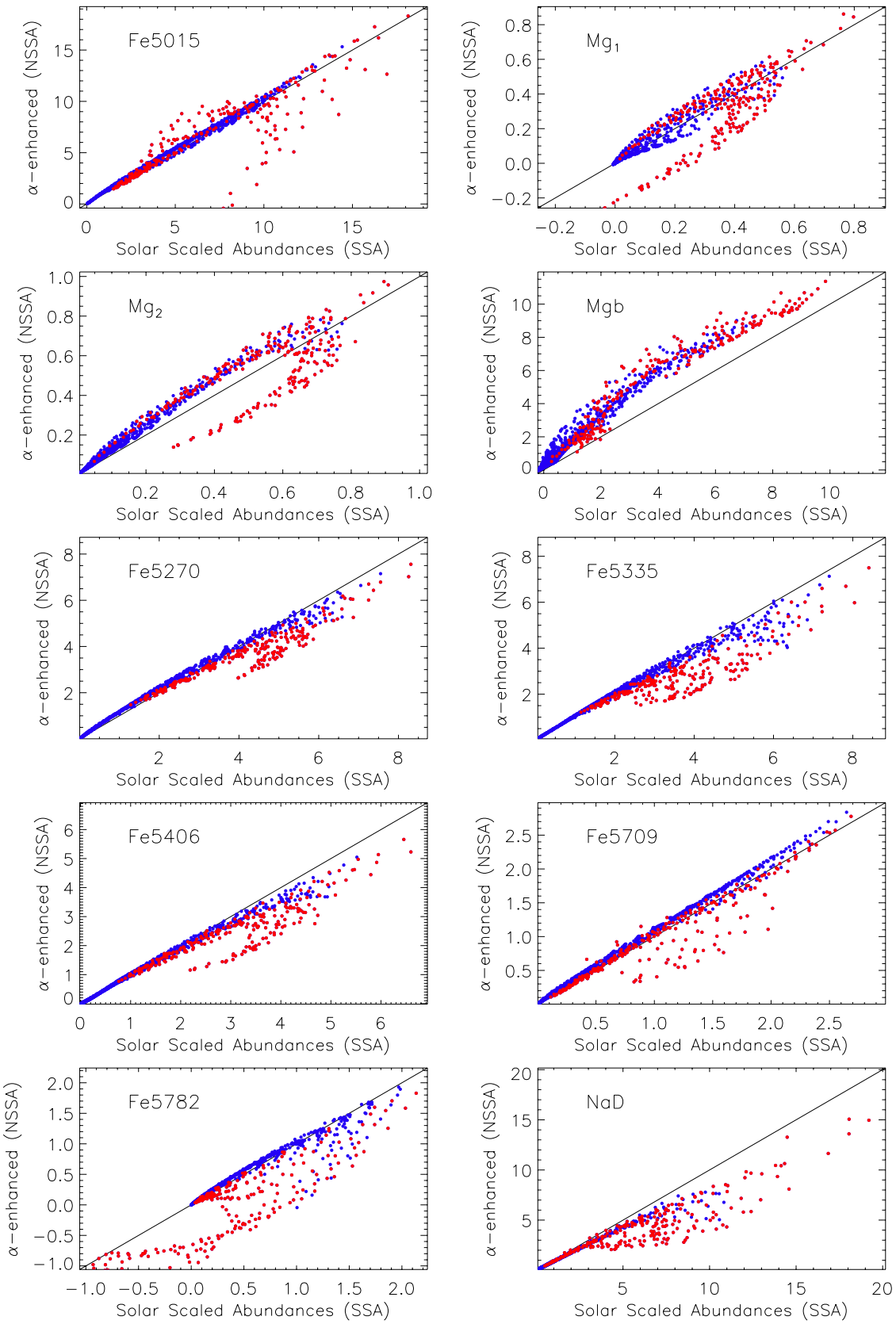

Figure 1. (Continued)

artifacts due to the presence of strong absorptions in the blue pseudo-continuum band for the corresponding synthetic spectra. The low NSSA values of CN_1, CN_2, and Fe4668 with respect to the SSA ones can be explained by the increase of CO, due to the higher O abundance, which causes a decrease of both CN and C_2. The Mg_1 index

shows a significant dispersion around the 45° line due to the combined effect of stronger Mg and weaker C_2 features in the NSSA spectra.

2. *The intermediate group*. This group contains six indices, namely, Fe4383, Fe5270, Fe5335, Fe5406, Fe5709, and Na D which show only marginal differences between NSSA and SSA values, mostly confined at the lowest temperatures.
3. *The* [α/Fe] *quasi-independent group*. This group contains six indices, namely, G4300, Ca4455, Fe4531, Hβ, Fe5015, and Fe5782 which do not show significant differences between NSSA and SSA values. The presence in this group of Ca4455 is not surprising since this index, which was supposed to measure the strength of a Ca I line, was actually found to be the most element-enhancement-free Lick index by Lee et al. (2009, see their Figure 8).

As far as the indices computed for $T_{\rm eff} < 4250$ K (indicated with red dots in Figure 1) are concerned we recall that the validity of the models and of the synthetic spectra decreases toward lower $T_{\rm eff}$ due to the incompleteness of the list of molecular species in the ODFs. Therefore, the accuracy of our synthetic indices may be somewhat poor. In any case, we can distinguish two groups.

1. The first group, which contains the five indices CaHK, Ca4227, G4300, Ca4455, and Mgb, shows a behavior which is only marginally different from that one at higher temperatures.
2. The second group contains the remaining 15 indices which fall, at least partially, in significantly different positions in the diagrams with respect to those at higher temperatures.

2.4. Calibration of Synthetic Indices

The comparison of synthetic indices with those measured on observed spectra requires, in general, a transformation from the synthetic system to the observational one (see, for example, Chavez et al. 2007). Therefore, to calibrate our system we looked for a sample of reference stars with reliable atmospheric parameter estimates in the ELODIE (Moultaka et al. 2004), INDO–U.S. (Valdes et al. 2004), and MILES (Cenarro et al. 2007) spectral libraries.

3. THE ELODIE, INDO–U.S., AND MILES DATA SET

From the merge of ELODIE,[9] INDO–U.S., and MILES spectral libraries, we selected 1598 spectra of stars with nominal parameters within the limits of our synthetic grids. Then, from this selection we excluded objects whose object-type identification in the CDS–SIMBAD database (hereafter CDS) indicated some kind of peculiarity (spectroscopic binaries, variable, etc.) leading to a final test set of 1232 stars (hereafter the EIM sample).

Lick/SDSS indices were computed from the spectra of the EIM sample after correcting the spectra for radial velocities and degrading their resolution at $R = 1800$.[10] Observational uncertainties on the computed indices were evaluated by using stars present in more than one stellar library and the need of zero-point corrections among the three different original spectral libraries was ruled out.

The obtained uncertainty values for each index are compared in Table 1 with the Lick/IDS error from WFGB94: the Lick/SDSS errors show a behavior similar to that of Lick/IDS ones with respect to the different indices but are significantly smaller due to the better internal consistency and quality of the EIM spectra.

Table 1
EIM Index Errors

Index	Units	Lick/IDS WFGB94	Lick/SDSS
CaHK	Å	...	1.316
CN1	mag	0.021	0.013
CN2	mag	0.023	0.013
Ca4227	Å	0.27	0.07
G4300	Å	0.39	0.14
Fe4383	Å	0.53	0.21
Ca4455	Å	0.25	0.06
Fe4531	Å	0.42	0.10
Hβ	Å	0.22	0.10
Fe5015	Å	0.46	0.16
Mg_1	mag	0.007	0.007
Mg_2	mag	0.008	0.008
Mgb	Å	0.23	0.08
Fe5270	Å	0.28	0.09
Fe5335	Å	0.26	0.09
Fe5406	Å	0.20	0.08
Fe5709	Å	0.18	0.06
Fe5782	Å	0.20	0.05
NaD	Å	0.24	0.14

Indications of deviations from solar partition abundances were searched in the literature and [α/Fe] estimates based on [Mg/Fe], [Si/Fe], and [Ti/Fe] were obtained, when available, from Borkova & Marsakov (2005) or from Valenti & Fischer (2005). Since several of our indices significantly depend on surface gravity, making it difficult to disentangle the effect of log g from that of [α/Fe], we decided to double check the log g values given in the spectral libraries with those calculated from *Hipparcos* parallaxes. New log g_H values were derived from the stellar $T_{\rm eff}$, [Fe/H], V_0, and parallax by using a "web interface for Bayesian estimation of stellar parameters"[11] (L. Girardi 2009, private communication). Eventually, a list of 333 "bona fide" stars was obtained by imposing the condition $|\log g - \log g_H| < 0.1$ dex. This list contains a sub-sample of 154 "SSA dwarf" stars (i.e., those with [α/Fe] values within $\pm$0.15 dex and $\log g > 3.5$) and 44 "giant" stars ($\log g < 3.5$) for which no estimates of [α/Fe] were found. By using these 198 stars we derived a set of transformation coefficients by performing linear regressions between the observed indices and the corresponding synthetic ones at the proper atmospheric parameter values. The synthetic indices were derived either from our SSA grid for "dwarfs" and metal rich "giants" ([Fe/H] > -0.5) or from the NSSA grid for metal poor "giants." For all indices, but Fe4668, the slopes of the linear fits were close to one, giving us confidence on the consistency between theoretical and observed spectra. Eventually, the derived coefficients were used to convert both the SSA and NSSA grids of synthetic indices into the observational Lick/SDSS system with the only exception of the Fe4668 index which, to be conservative, was excluded. We stress that we preserve the intrinsic differences between the uncalibrated SSA and NSSA grids since a unique set of transformation coefficients is used to calibrate both grids.

[9] Only stars with good quality flags for all the atmosphere parameters were selected.
[10] These indices are available from the authors upon request.
[11] http://stev.oapd.inaf.it/cgi-bin/param

3.1. Comparison between Synthetic and Observed Indices

A direct comparison between calibrated synthetic indices and observed ones requires the knowledge of all the atmospheric parameters (i.e., $T_{\rm eff}$, log g, [Fe/H], and [α/Fe]) for each star in order to compare like with like. Unfortunately, both systematic and random errors affect the estimates of $T_{\rm eff}$, log g, [Fe/H], and [α/Fe] present in the literature. In the following, we decided to use $T_{\rm eff}$ as the baseline for the comparison since this is the most important and less model-dependent parameter. It must be recalled that, when generating synthetic stellar spectra, stellar atmosphere models give rise to some intrinsic temperature scale. On the other hand, a specific temperature scale must be adopted for interpreting observed spectra in order to determine physical parameters of the stars. These two different approaches may, therefore, introduce mismatches between the temperature scales of the synthetic and of the observed spectra. In the following, we assume that stars and synthetic spectra are on the same $\theta = 5040/T_{\rm eff}$ temperature scale and we check the validity of this assumption by studying the behavior of the synthetic and observational Hβ index. In fact, Hβ is a temperature indicator almost independent of surface gravity, metallicity, and α enhancement. Then, we separate the stars in two groups of log g to represent "dwarf" and "giant" stars (log $g = 4.5 \pm 0.5$ and log $g = 2.5 \pm 0.5$, respectively) and we perform the comparison separately in different [Fe/H] bins whose amplitude ($\pm$0.1 dex) should take into account the uncertainties affecting the estimates of stellar metallicity.

Out of the 1232 stars in the EIM sample, 541 and 391 stars have log g estimates consistent, according to our criteria, with those of "dwarf" and "giant" stars, respectively.

For each of the 19 indices the observed values are plotted versus θ for the two groups of stars together with SSA and NSSA isogravities of calibrated synthetic indices in eight different panels corresponding to intervals of Δ[Fe/H] = $\pm$0.1 dex centered at $-2.5, -2.0, -1.5, -1.0, -0.5, 0.0, +0.2$, and +0.5. For the H$\beta$ index Figures 2 and 3 show the absence of any systematic offset between the observational point positions and the synthetic isogravities. This good agreement confirms that stars and synthetic spectra are on the same $\theta = 5040/T_{\rm eff}$ temperature scale and allow us to be confident on the methodology adopted for the comparison. Other examples of the comparison are shown in Figures 4–9 for Fe5270, CaHK, and Mgb indices. The overall good agreement of the observational points with the isogravities for both "dwarfs" and "giants" indicates the correctness of the behavior of our synthetic indices versus surface gravity. Moreover, the good agreement in all the [Fe/H] panels of Figures 2–5 shows that the dependency of observational indices on metallicity is also well reproduced by our synthetic indices. As far as the [α/Fe] behavior is concerned, the plots in Figures 6–9 indicate, as expected on the basis of literature results, that the loci of the observational points get closer to the prediction of NSSA (i.e., α-enhanced) indices as metallicity decreases.

In what follows more details on the results of the comparison are discussed separately for "dwarf" and "giant" stars.

3.1.1. "Dwarf" Stars

The agreement between calibrated synthetic indices and the observed ones is very good in all the 19 indices for almost all of the 541 stars only with a few outliers which will be discussed later on and in the Appendix A.1. The observed points fall, in general, between the isogravities corresponding to log $g = 5.0$ and log $g = 4.0$ dex taking into account observational uncertainties.

There are clear indications of some α enhancement in the diagram of the [α/Fe] sensitive group indices at lower metallicity since the data move from the SSA isogravities toward the NSSA ones for [Fe/H] $\leqslant 0$ (see, for example, Figures 6–9).[12]

A sound comparison at effective temperature lower than 4250 K and/or at very low metallicity ([Fe/H] $\leqslant -1.5$) is hampered by the few data points available in the EIM sample.

Appendix A.1 contains a discussion of the few (48) outliers for which the observational points for some of the indices fall at a distance from the isogravities larger than typical observational errors. Out of the 48 stars, 37 are outliers only for a few randomly distributed indices (see Table 2) and their anomalies may be attributed to artifacts in the observed spectra in the corresponding index regions. In particular, we notice that discrepancies in CaHK, found in 20 of these 37 stars, are mainly due to the decrease in S/N in the observed spectra toward shorter wavelengths. Concerning the remaining 11 stars, Appendix A.1 shows that eight out of the 11 outliers may be explained by assuming errors in the estimates of their atmospheric parameters given in the stellar libraries. As far as the other three stars are concerned, the discrepancies may be due to intrinsic stellar peculiarities (HD223524) or to potential inaccuracies of our synthetic spectra at $T_{\rm eff} < 4000$ K (see Section 4.2).

3.1.2. "Giant" Stars

In comparing the observed indices of the 391 "giant" stars in our test sample with synthetic isogravities, we must recall that our calibration for giant gravities is less accurate than that for dwarf gravities. In fact the number of "giants" in our calibration set is less than one-third of the number of "dwarfs" and no individual estimates of [α/Fe] are available. Nevertheless the agreement between the loci of the observational points and synthetic isogravities is quite good. There is only a slight tendency of the synthetic Fe4531, Mg1, Mg2, and Fe5709 to be overestimated at [Fe/H] $\geqslant +0.2$. We also notice some discrepancy for CaHK at [Fe/H]$\sim$+0.2 which may be explained by the decrease in S/N in the observed spectra toward shorter wavelengths. As in the case of the "dwarfs," a sound comparison at effective temperature lower than 4250 K and/or at very low metallicity ([Fe/H] $\leqslant -1.5$ is hampered by the few data points available in our test sample.

We identified 22 outliers (see Table 2) but only three of them, discussed in Appendix A.2, have more than five of the observational indices inconsistent with those predicted from the SSA and NSSA grids on the basis of their atmospheric parameters. As in the case of "dwarf" outliers it is very likely that these three stars have inaccurate atmospheric parameter values listed in the MILES spectral library.

In conclusion, we notice that, even if our modeling of giant spectra is less accurate than in the case of "dwarfs" (for instance, our computations ignore any effect of mixing on surface chemical composition), our calibrated synthetic indices give a good representation of observations also in this luminosity class.

4. THE SDSS–DR7 SAMPLE

A fundamental step from the observational point of view in the knowledge of the Milky Way stellar content has been accom-

[12] The relative paucity of α-enhanced stars is due to the presence in the ELODIE, INDO–U.S., and MILES stellar libraries of mostly SSA stars as already showed by Franchini et al. (2005).

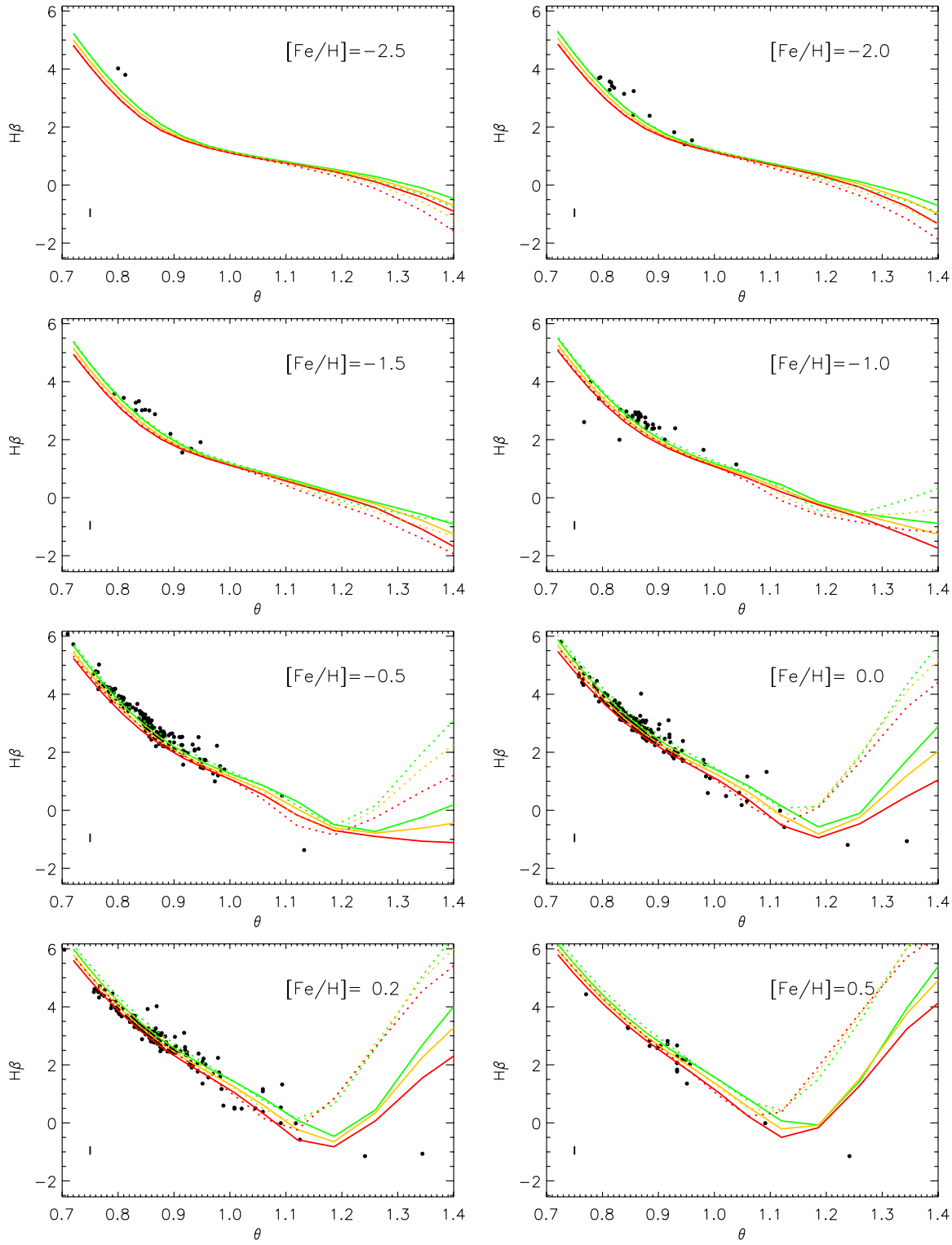

Figure 2. Spectral index Hβ of EIM "dwarf" stars vs. $\theta = 5040/T_{\rm eff}$ in different metallicity groups. Synthetic SSA (solid lines) and NSSA (dotted lines) isogravities are overplotted: log $g = 4.0$ (green), log $g = 4.5$ (yellow), and log $g = 5.0$ (red). Vertical bar in the left-lower corner represents observational uncertainty.
(A color version of this figure is available in the online journal.)

plished with the SDSS (York et al. 2000), since its photometric and spectroscopic stellar database (Abazajian et al. 2009; DR7) represents the most extended collection of optical data available to date. SDSS data have been the subject of analyses in a large number of studies, mostly devoted to galaxies, quasars, and peculiar objects for which the survey was primarily designed.

In spite of the limited resolution and widely variable quality of SDSS spectra, and the limitation due to strong biases in magnitude, color, and sky coverage, this enormous stellar data set represents a valuable tool for deriving statistical information about chemical and dynamical properties of the stellar populations of the Galaxy.

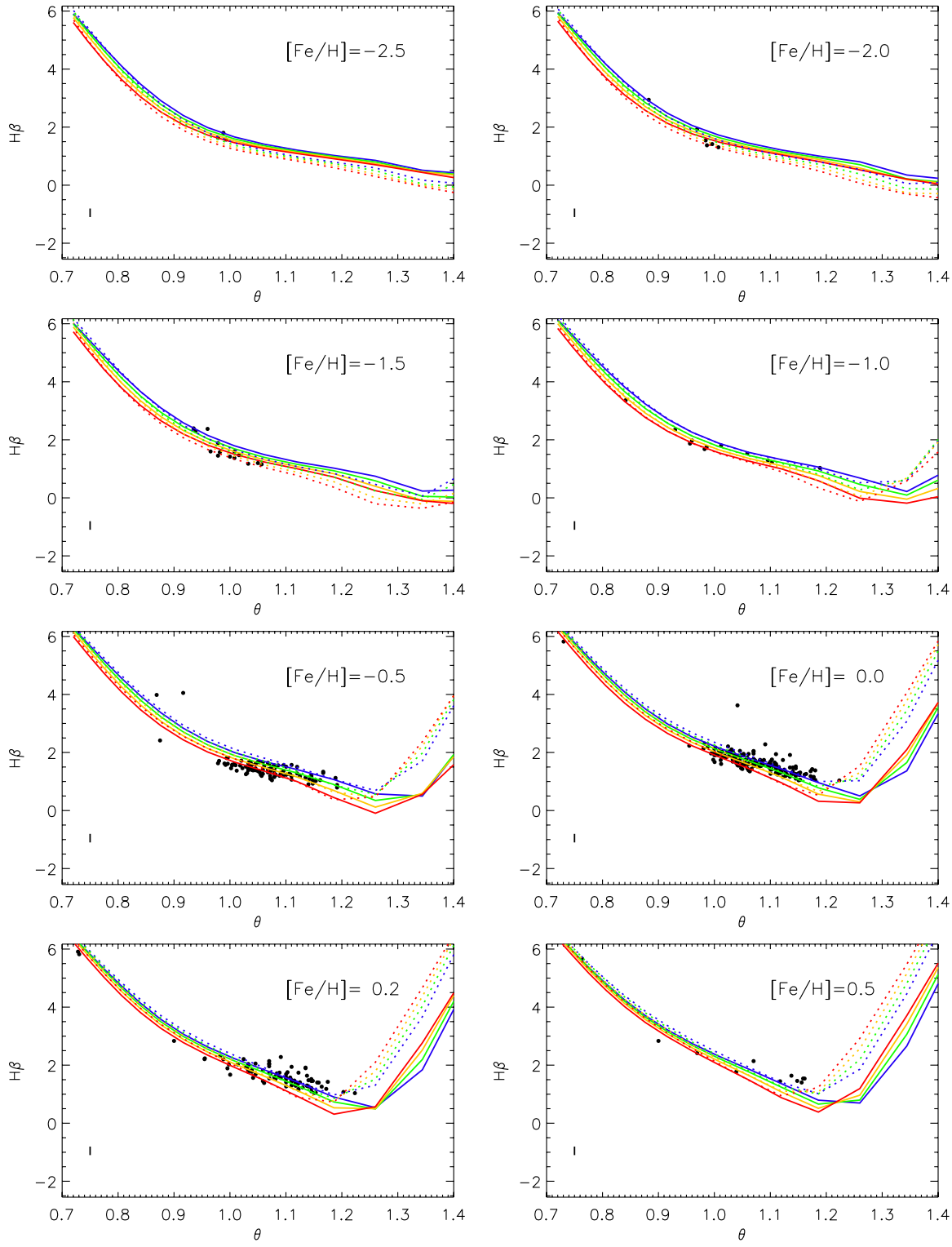

Figure 3. Spectral index Hβ of EIM "giant" stars vs. $\theta = 5040/T_{\rm eff}$ in different metallicity groups. Synthetic SSA (solid lines) and NSSA (dotted lines) isogravities are overplotted: $\log g = 2.0$ (green), $\log g = 2.5$ (yellow), and $\log g = 3.0$ (red). Vertical bar in the left-lower corner represents observational uncertainty.
(A color version of this figure is available in the online journal.)

Among the studies devoted to "normal" stars, Jurić et al. (2008) attempted a full modeling of Galactic components from photometric parallaxes for 48 million stars by analyzing the derived Galactic three-dimensional number density distribution. Allende Prieto, Beers, Rockosi, and collaborators provide extended examples of results obtainable from the analysis of SDSS stellar spectra via Principal Component Analysis (Re Fiorentin et al. 2007) and/or Wavelength Range Selection method (Allende Prieto et al. 2006, hereafter AP06; Carollo et al. 2007). In the following, we compare computed Lick/SDSS indices of a sample of about 18,000 late F, G, and K stars from the DR7 spectroscopic database with the predictions of

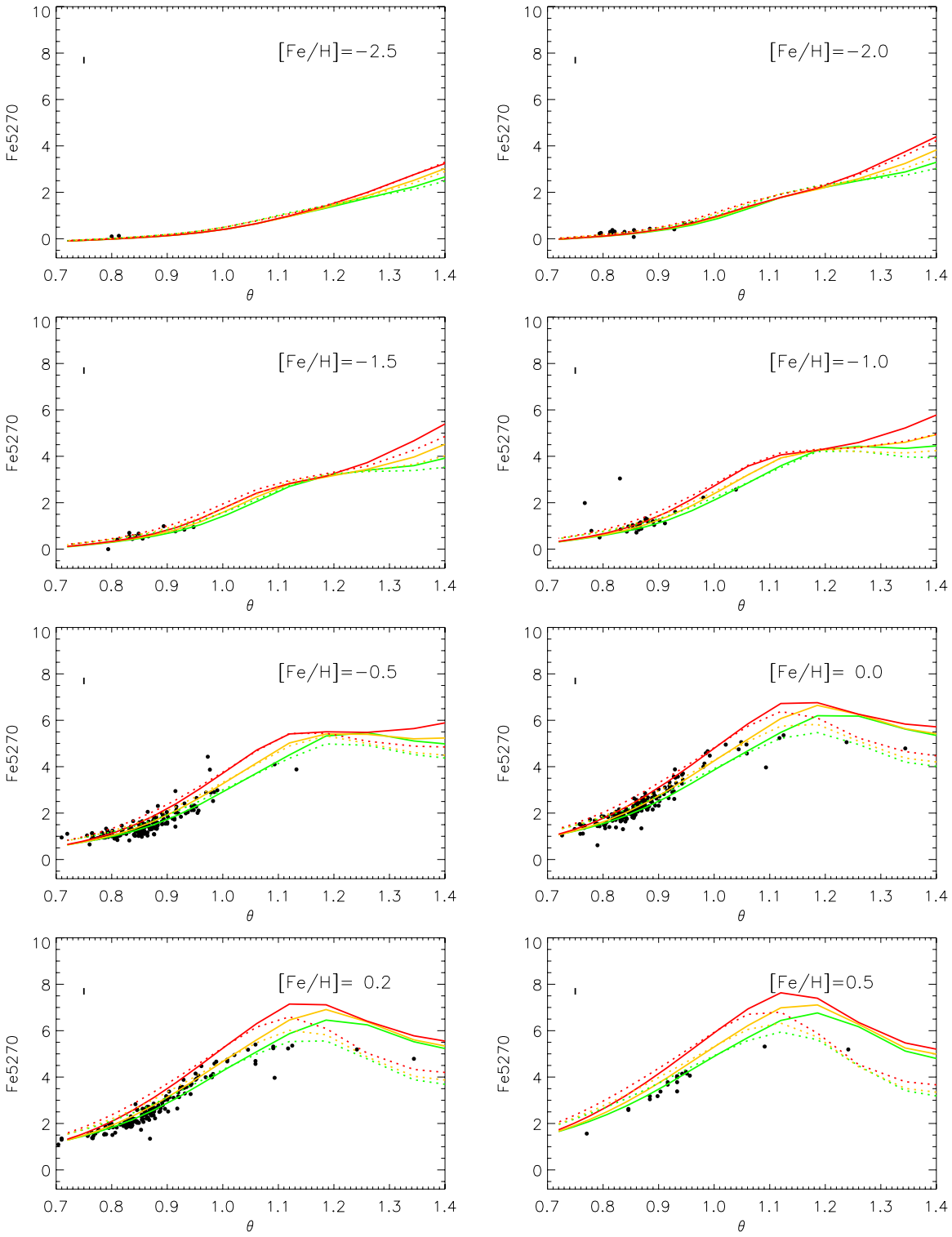

Figure 4. Spectral index Fe5270 of EIM "dwarf" stars vs. $\theta = 5040/T_{\rm eff}$ in different metallicity groups. Synthetic SSA (solid lines) and NSSA (dotted lines) isogravities are overplotted: $\log g = 4.0$ (green), $\log g = 4.5$ (yellow), and $\log g = 5.0$ (red). Vertical bar in the left-upper corner represents observational uncertainty. (A color version of this figure is available in the online journal.)

our synthetic indices in order to extend the analysis presented in Section 3.

4.1. Screening of the DR7 Database

The observational data set was extracted from the seventh SDSS Data Release (SDSS–DR7; Abazajian et al. 2009), which contains spectra for approximately 380,000 objects classified as stars (http://www.sdss.org/dr7/) earlier than M type. The DR7 data are distributed via the Catalog Archive Server (CAS), a Structured Query Language (SQL) database with fast search capabilities, and the Data Archive Server (DAS) which contains the output of the spectroscopic reduction pipelines. The SDSS data retrieval is therefore a twofold process: (1) define an SQL query to search the CAS database for all objects that meet

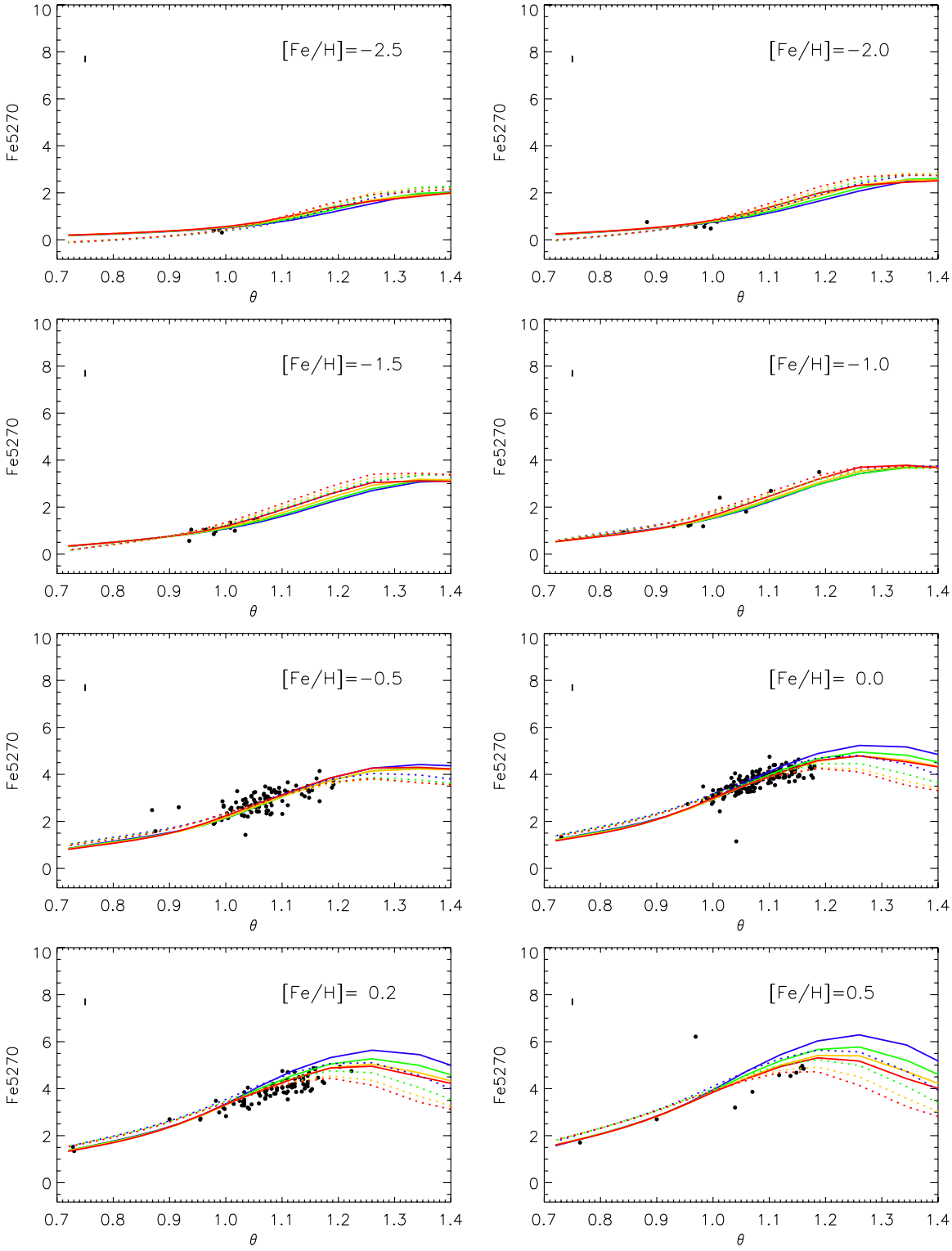

Figure 5. Spectral index Fe5270 of EIM "giant" stars vs. $\theta = 5040/T_{\rm eff}$ in different metallicity groups. Synthetic SSA (solid lines) and NSSA (dotted lines) isogravities are overplotted: log $g = 1.5$ (blue), log $g = 2.0$ (green), log $g = 2.5$ (yellow), and log $g = 3.0$ (red). Vertical bar in the left-upper corner represents observational uncertainty.

(A color version of this figure is available in the online journal.)

specified criteria; and (2) use the obtained list to retrieve the spectra. To run the SQL query we used the CasJobs Batch Query Services which, as a result of the submitted query, creates a table containing the columns specified by the clause.

From the total set of 380,214 SDSS–DR7 spectra classified as STARS we selected late F, G, and K stellar-type spectra by adopting the following constraints on photometric data: $0.3 < g - r < 1.3$ mag and $(g + r)/2 < 23$ mag. After discarding spectra with null signal, we obtained a list of 38,327 spectra for which SDSS photometry is available. A first-order check on the quality of the calibration of each spectrum was performed by comparing the spectrophotometric magnitudes

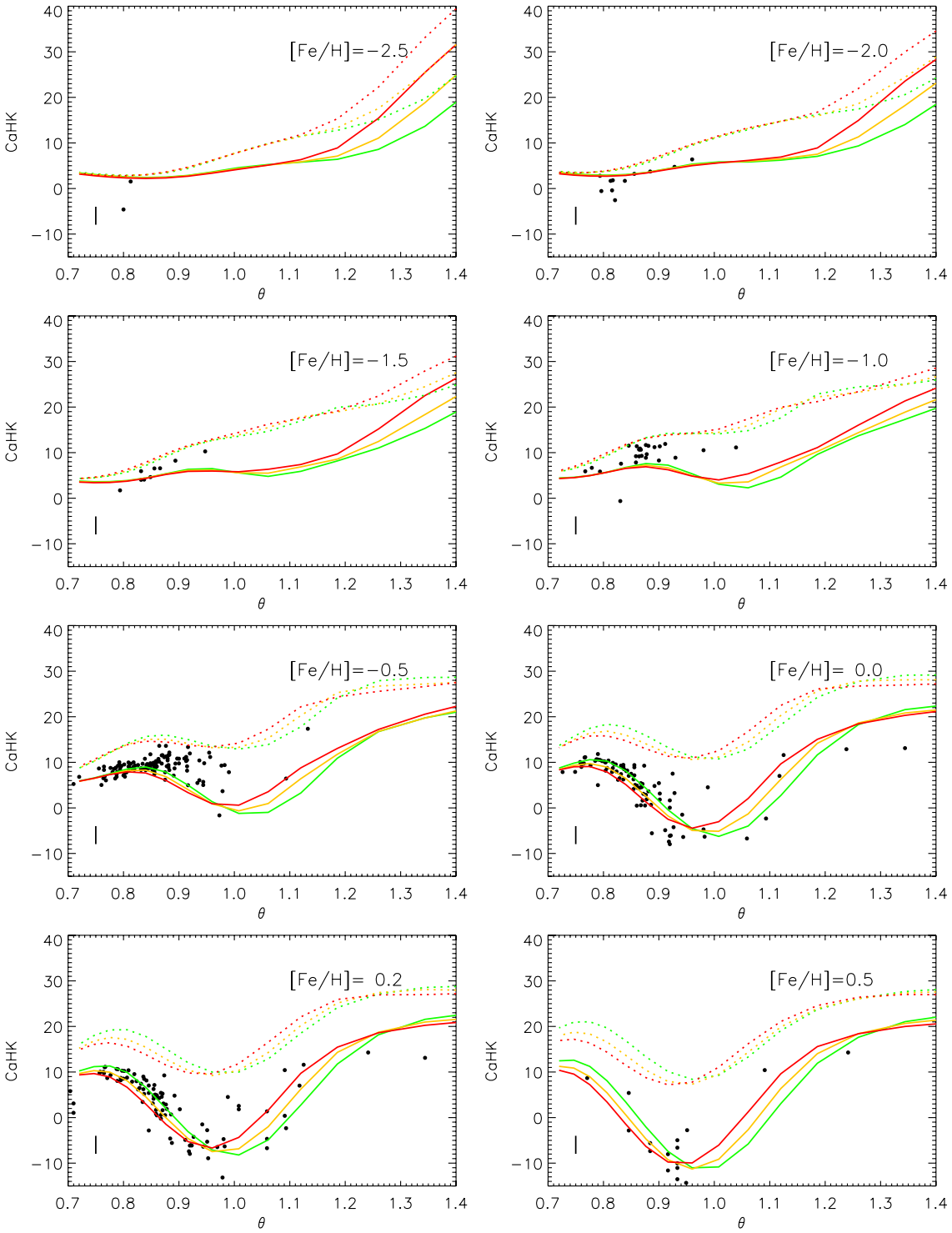

Figure 6. Spectral index CaHK of EIM "dwarf" stars vs. $\theta = 5040/T_{\rm eff}$ in different metallicity groups. Synthetic SSA (solid lines) and NSSA (dotted lines) isogravities are overplotted: $\log g = 4.0$ (green), $\log g = 4.5$ (yellow), and $\log g = 5.0$ (red). Vertical bar in the left-lower corner represents observational uncertainty.
(A color version of this figure is available in the online journal.)

$(g_{\rm sp}, r_{\rm sp}, i_{\rm sp})$[13] and relative colors $(g-r)_{\rm sp}$, $(r-i)_{\rm sp}$ with the corresponding photometric "point-spread function (PSF)" magnitudes and colors.

We applied an iterative procedure which discards objects with absolute difference in magnitudes and colors greater than the 3σ values of the distributions of differences and found 27,776 objects with

$$|g_{\rm sp} - g_{\rm PSF}| \leqslant 3 \times 0.10 \ \ {\rm mag}$$
$$|r_{\rm sp} - r_{\rm PSF}| \leqslant 3 \times 0.09 \ \ {\rm mag}$$
$$|i_{\rm sp} - i_{\rm PSF}| \leqslant 3 \times 0.12 \ \ {\rm mag}$$
$$|(g-r)_{\rm sp} - (g-r)_{\rm PSF}| \leqslant 3 \times 0.06 \ {\rm mag}$$
$$|(r-i)_{\rm sp} - (r-i)_{\rm PSF}| \leqslant 3 \times 0.04 \ {\rm mag}.$$

[13] Computed by the SDSS Data Reduction Pipeline and given in the FITS header of the released spectra.

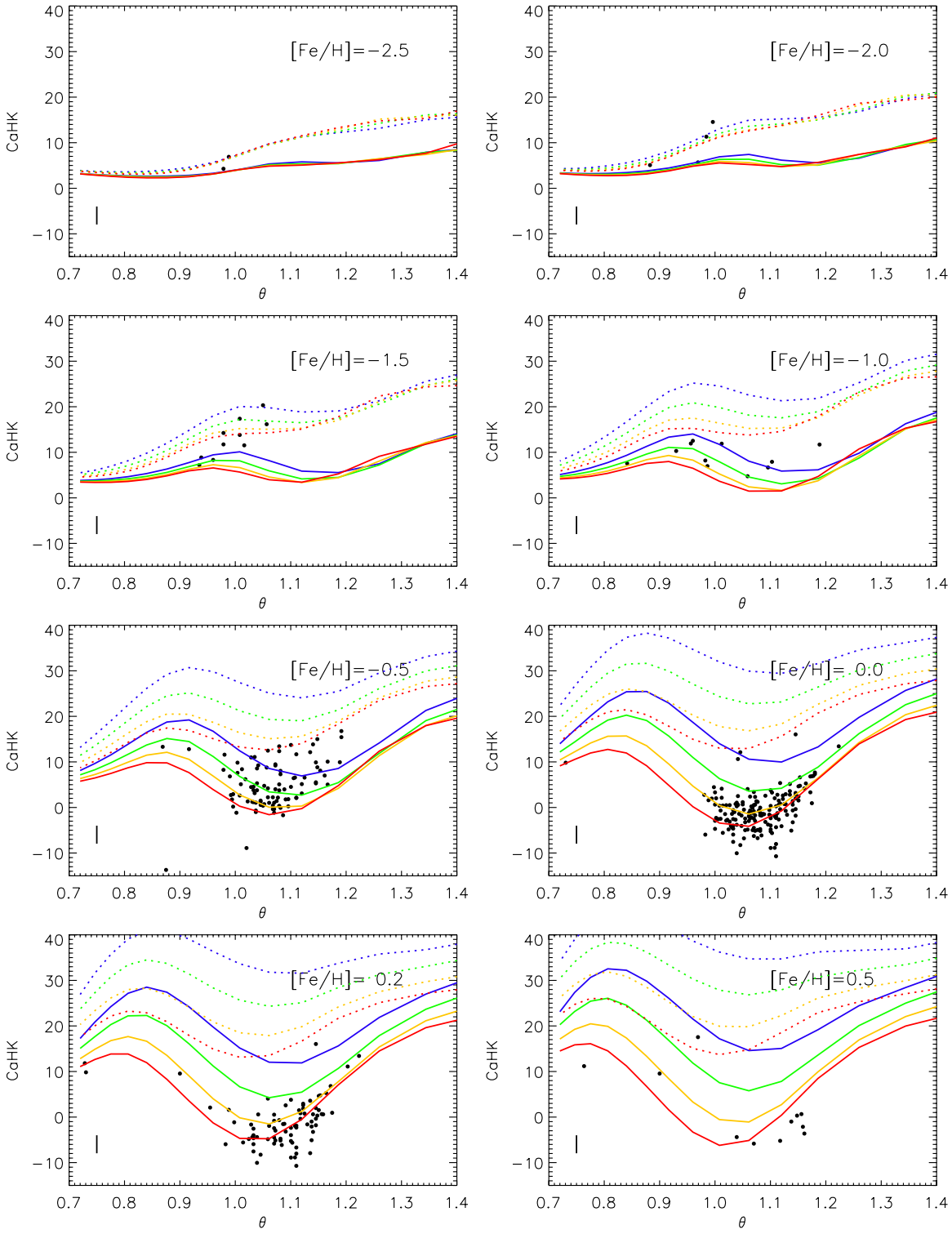

Figure 7. Spectral index CaHK of EIM "giant" stars vs. $\theta = 5040/T_{\rm eff}$ in different metallicity groups. Synthetic SSA (solid lines) and NSSA (dotted lines) isogravities are overplotted: log $g = 1.5$ (blue), log $g = 2.0$ (green), log $g = 2.5$ (yellow), and log $g = 3.0$ (red). Vertical bar in the left-lower corner represents observational uncertainty.

(A color version of this figure is available in the online journal.)

Figure 10 represents the color–color diagram of the "PSF" colors for these 27,776 objects together with two sequences of theoretical colors from "Grids of color indices from ATLAS9 model atmospheres."[14] The two reference sequences mark the theoretical region of dwarf G–K stars and refer to effective temperatures, $T_{\rm eff}$, in the range 4250–6500 K, surface gravity log $g = 4.5$, and overall metallicity [M/H] $= -4.0$ (filled circles) and +0.5 (filled triangles), respectively. The figure shows an overall consistency of observed colors with those predicted for main-sequence stars of spectral types G and K. A conservative

[14] http://wwwuser.oat.ts.astro.it/castelli/colors.html

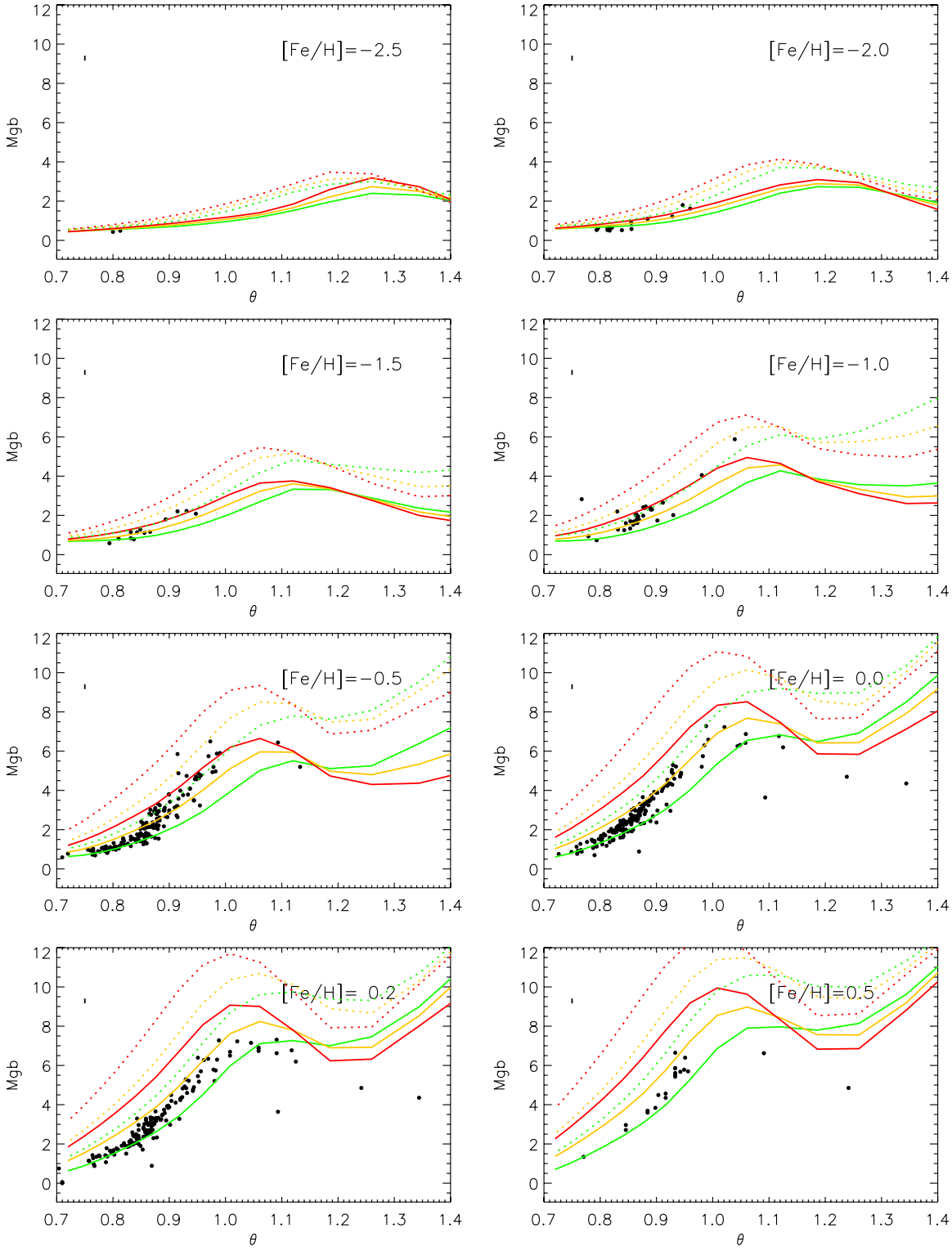

Figure 8. Spectral index Mgb of EIM "dwarf" stars vs. $\theta = 5040/T_{\rm eff}$ in different metallicity groups. Synthetic SSA (solid lines) and NSSA (dotted lines) isogravities are overplotted: $\log g = 4.0$ (green), $\log g = 4.5$ (yellow), and $\log g = 5.0$ (red). Vertical bar in the left-upper corner represents observational uncertainty.
(A color version of this figure is available in the online journal.)

removal of outliers was performed by excluding objects outside a strip centered on the sequence of the bulk of data; 99% of objects fall between the two boundaries of the strip and the remaining 1% are excluded from further processing.

The selected 27,503 spectra were analyzed for deriving radial velocity estimates, $v_{\rm rad}$, by using the *fxcor* IRAF task. We considered eight partially overlapping 500 Å wide intervals starting from $\lambda = 4000$ Å with step size $\Delta\lambda = 250$ Å and, for each interval, we derived a value of $v_{\rm rad}$ by cross-correlating the observations with a template synthetic spectrum (see Section 2). The derived $v_{\rm rad}$ was considered reliable if the standard deviation of the values from the eight wavelength intervals was less

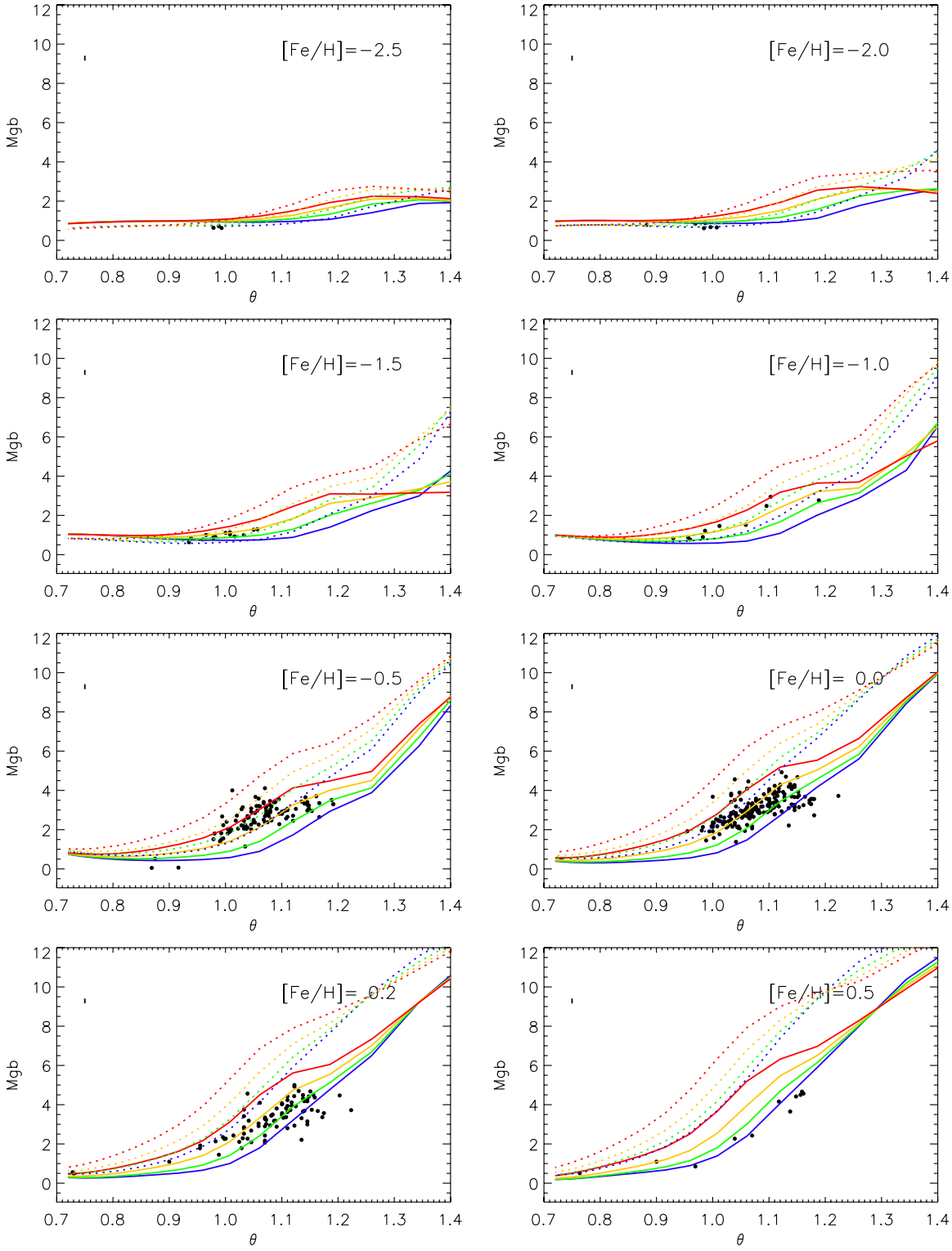

Figure 9. Spectral index Mgb of EIM "giant" stars vs. $\theta = 5040/T_{\rm eff}$ in different metallicity groups. Synthetic SSA (solid lines) and NSSA (dotted lines) isogravities are overplotted: log $g = 1.5$ (blue), log $g = 2.0$ (green), log $g = 2.5$ (yellow), and log $g = 3.0$ (red). Vertical bar in the left-upper corner represents observational uncertainty.

(A color version of this figure is available in the online journal.)

than 30 km s^{-1}, leading to a set of $\langle v_{\rm rad}\rangle$ determinations for 17,600 spectra (with $|v_{\rm rad}|$ less than 460 km s^{-1}, i.e., less than the Milky Way escape velocity). The correlation between the two sets of determinations appears very tight and a detailed check on the spectra of the only three outliers (with differences between SDSS and our values in excess of 150 km s^{-1}) confirms the validity of our determinations. The semi-external error, $\sigma(v_{\rm radSDSS} - <v_{\rm rad}>) = 15$ km s^{-1}, is consistent with the mean internal error of our estimates.

In order to evaluate the quality of the spectra, an estimate of the average S/N was computed for each spectrum by using the median value of the ratio between the signal and its standard

Table 2
Outliers

Star	$T_{\rm eff}$ (K)	log g	$[\frac{\rm Fe}{\rm H}]$	$[\frac{\alpha}{\rm Fe}]$	CaHK (Å)	CN1 (mag)	CN2 (mag)	Ca4227 (Å)	G4300 (Å)	Fe4383 (Å)	Ca4455 (Å)	Fe4531 (Å)	Hβ (Å)	Fe5015 (Å)	Mg_1 (mag)	Mg_2 (mag)	Mgb (Å)	Fe5270 (Å)	Fe5335 (Å)	Fe5406 (Å)	Fe5709 (Å)	Fe5782 (Å)	NaD (Å)
"Dwarf" Stars																							
G176-11[I]	3544	4.85	−1.45			X	X		X	X			X		X	X		X	X	X			X
HD111631[M]	3750	4.75	0.10		X			X	X		X	X	X	X			X		X			X	
HD157881[M]	4060	4.57	0.38					X	X		X		X	X		X	X						
HD237903[I]	4070	4.70	0.00					X	X		X		X			X	X						
BD+062986[M]	4450	4.80	−0.30			X	X		X	X			X								X		
HD223524[M]	4610	4.30	0.07			X	X	X			X	X			X	X	X	X	X				X
HD21197[M]	4620	4.59	0.30						X														
HD82106[E]	4827	4.10	−0.11			X	X																
G161-29[I]	5100	4.30	0.10	0.05											X								
HD75732[I]	5150	4.15	0.29	0.09	X																		
G125-04[I]	5160	4.43	−0.62											X					X	X		X	
BD+151305[M]	5180	4.10	−0.60		X	X	X			X	X	X		X				X	X	X	X	X	X
HD77338[M]	5290	4.75	0.26		X																		
G180-35[I]	5310	4.40	0.46		X										X								
HD99491[I]	5340	4.40	0.16		X	X																	
HD115589[I]	5400	4.54	0.40	−0.10											X								
G163-78[I]	5400	4.20	0.45		X									X							X		
G102-27[I]	5420	4.00	−1.05											X									
HD173701[I]	5423	4.40	0.18	0.00		X																	
G200-36[I]	5470	4.70	0.06		X																		
HD159909[E]	5479	4.10	0.06	0.06		X	X																
HD104304[I]	5480	4.24	0.18	−0.02	X	X																	
G175-33[I]	5490	4.50	0.13		X																		
G103-68[I]	5510	4.00	−0.63			X	X	X	X		X	X			X	X				X	X		X
HD188510[E]	5510	4.56	−1.56	0.23											X								
HD180890[I]	5530	4.53	0.14		X																		
HD80607[E]	5579	4.34	0.36			X	X																
HD89010[E]	5667	4.00	−0.05								X												
HD49178[I]	5680	4.45	0.01		X																		
HD186408[I]	5800	4.26	0.06	0.04										X			X	X	X				
HD88986[E]	5823	4.10	0.01												X								
HD134169[I]	5830	4.11	−0.83	0.31		X	X																
HD84737[E]	5889	4.12	0.06												X								
G012-21[I]	5940	4.23	−1.33				X																
HD68988[I]	5960	4.25	0.37		X																		

Table 2
(Continued)

Star	$T_{\rm eff}$ (K)	log g	$[\frac{\rm Fe}{\rm H}]$	$[\frac{\alpha}{\rm Fe}]$	CaHK (Å)	CN1 (mag)	CN2 (mag)	Ca4227 (Å)	G4300 (Å)	Fe4383 (Å)	Ca4455 (Å)	Fe4531 (Å)	Hβ (Å)	Fe5015 (Å)	Mg_1 (mag)	Mg_2 (mag)	Mgb (Å)	Fe5270 (Å)	Fe5335 (Å)	Fe5406 (Å)	Fe5709 (Å)	Fe5782 (Å)	NaD (Å)
HD76813[I]	6070	4.20	−0.82		X	X	X		X	X	X	X	X	X	X	X		X	X	X	X	X	X
G140-05[I]	6140	4.31	−2.15		X																		
G183-11[I]	6180	4.00	−2.11		X																		
BD+241676[M]	6200	4.38	−2.45	0.32	X				X						X								
G048-29[I]	6300	4.00	−2.66		X				X														
G165-39[I]	6330	4.03	−1.96		X																		
G119-64[I]	6350	4.79	−1.15												X								
G245-32[I]	6350	4.48	−1.62		X																		
HD92769[I]	6380	4.10	−0.15			X	X		X	X	X	X		X					X				
HD121258[M]	6570	4.00	−0.92			X	X	X	X	X	X	X	X	X	X	X	X	X	X	X	X	X	X	X
HD78209[I]	7100	4.20	0.24		X				X			X											
HD8829[M]	7160	4.15	0.25		X				X			X		X									
HD103877[M]	7340	4.00	0.40		X	X	X				X	X											
"Giant" Stars																							
HD113092[I]	4240	2.11	−0.83			X	X					X											
HD112127[M]	4580	2.07	0.13												X				X	X			
HD39003[E]	4593	2.14	−0.09																		X		
HD135482[M]	4620	2.57	0.13						X														
HD81192[E]	4688	2.58	−0.64												X								
HD105740[M]	4700	2.50	−0.51																				X
HD82734[M]	4710	2.65	0.30												X					X			
HD210295[I]	4800	2.20	−1.34												X								
HD165634[M]	4820	2.76	−0.14						X						X								
HD10486[I]	4850	2.80	0.05							X					X	X			X	X			X
HD76294[I]	4850	2.50	0.38											X	X			X	X	X			
HD208110[I]	4870	2.10	−0.68							X								X			X		
HD110930[I]	4980	2.50	−0.18																		X		
G122-66[I]	4980	2.74	−0.48													X							
HD100906[M]	4980	2.00	−1.02						X														
HD12014[M]	5200	2.30	0.45							X	X	X						X	X	X		X	X
HD166161[I]	5270	2.51	−1.16			X	X																
HD119516[I]	5390	2.30	−1.55						X														
HD172365[M]	5800	2.12	−0.36								X	X	X	X				X	X				X
HD92125[I]	5600	2.10	0.38											X									
HD188650[M]	5760	2.90	−0.4		X	X	X		X														
HD2857[M]	7450	2.60	−1.6						X														

Notes.
[E] Atmospheric parameter values from ELODIE.
[I] Atmospheric parameter values from INDO–U.S.
[M] Atmospheric parameter values from MILES.

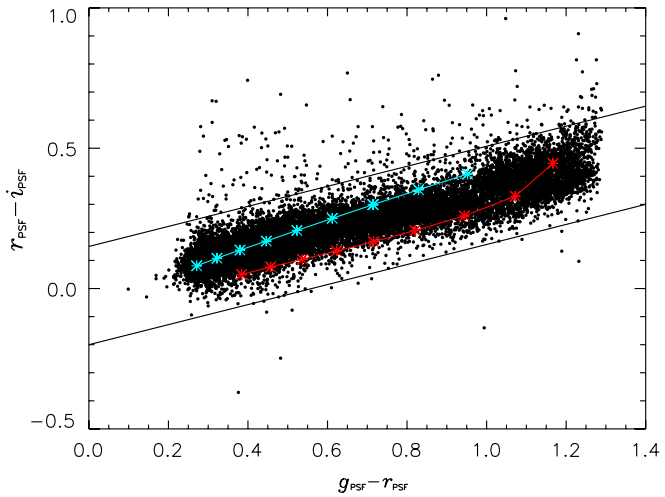

Figure 10. Color–color diagram. Two sequences of theoretical colors for $T_{\rm eff}$ in the range 4250–6500 K, log g = 4.5, and overall metallicity [M/H] = −4.0 (light blue) and +0.5 (red), respectively, are illustrated. The acceptance strip is limited by the two straight lines given by the following equations: $(r-i)_{\rm PSF} = 0.357(g-r)_{\rm PSF} + 0.15$ and $(r-i)_{\rm PSF} = 0.357(g-r)_{\rm PSF} - 0.20$. (A color version of this figure is available in the online journal.)

deviation given in the SDSS FIT files. The distribution of S/N values peaks at about S/N = 25.

Eventually, the SDSS spectra were corrected by using our determinations of radial velocity and Lick/SDSS indices were computed.

4.2. Comparison between Synthetic and Observed Indices

As already discussed in Section 3.1, a direct comparison between calibrated synthetic indices and the observed ones requires the knowledge of all the atmospheric parameters for each individual star.

SDSS–DR7 provides, through the table sppParams, individual estimates of $T_{\rm eff}$, log g, [Fe/H], and [α/Fe] derived using SEGUE Stellar Parameter Pipeline (SSPP; Lee et al. 2008). The table sppParams contains 11 estimates of effective temperature ($T1, \ldots, T11$), 10 estimates of surface gravity ($G1, \ldots, G10$), and 12 estimates of metallicity ($M1, \ldots, M12$) derived with different techniques. In six cases, $T6, \ldots, T11$, log g, and [Fe/H] are simultaneously derived with $T_{\rm eff}$, while in the other cases, $T1, \ldots, T5$, only $T_{\rm eff}$ is given.[15] Furthermore, the table provides weighted average values, $T_{\rm SSPP}$, $G_{\rm SSPP}$, and $M_{\rm SSPP}$ (see Lee et al. 2008 for full details).

First of all we investigate if there is an agreement between the temperature scale of our synthetic indices and any of the SSPP temperature determinations. Therefore, we start the comparison by analyzing the behavior of the index Hβ which is the best temperature indicator among the Lick/SDSS indices. Figures 11–13 show the comparison of the Hβ index values computed from SDSS spectra with synthetic ones. For each of the T_i (with $i = 1, \ldots, 11$) estimates we sorted the index values in θ after dividing them in groups of "dwarfs" and "giants" of different metallicity as in Section 3.1 by using the G_j and M_k associated values for $T6, \ldots, T11$ or the SSPP average values for $T1, \ldots, T5$. Due to the large number of points involved and to the lower S/Ns of SDSS spectra than those of ELODIE, INDO–U.S., and MILES ones we decided use median values instead of individual points as in Figures 2–9. Therefore, a running median on θ, Hβ, log g, and [Fe/H] was computed and, for the sake of clarity, only some of the median points (sampled at constant step) are plotted in Figures 11–13 together with their 68% confidence intervals (represented by error bars). Eventually, to get the theoretical counterpart of each median point, synthetic SSA and NSSA Hβ values were interpolated at each tern of median ($T_{\rm eff}$, log g, [Fe/H]) and overplotted as blue and red lines, respectively.

In all the cases the synthetic indices predict trends with θ that are qualitatively in agreement with the observed ones. On the other hand, it is clear that the result of the comparison is strongly dependent on the choice of the tern of parameter values. In particular, different systematic offsets appear at low or high temperatures and/or at different metallicity by using different stellar T_i estimates showing that none of the 11 SSPP temperatures is on the same temperature scale of the Lick/SDSS indices and of the EIM sample (see for comparison Figures 2 and 3). Moreover, the use of $G_{\rm SSPP}$, and $M_{\rm SSPP}$ for $T1, \ldots, T5$ introduces a further uncertainty due to inconsistency in the terns of parameter values, since $T_{\rm eff}$, log g, and [Fe/H] should be derived simultaneously to take into account their crosstalk. Among the six homogeneous terns the best agreement between observations and theoretical predictions for "dwarfs" is achieved by using the terns corresponding to

1. $T7$, $T8$, and $T9$ for [Fe/H]$\simeq -2.0$;
2. $T7$ for [Fe/H]$\simeq -1.5$;
3. $T6$ for [Fe/H]$\simeq -1.0$;
4. $T6$ and $T8$ for [Fe/H]$=\simeq -0.5$ at high and low temperatures, respectively;
5. $T8$ and $T11$ for [Fe/H]$\simeq 0.0$;
6. $T6$ and $T11$ for [Fe/H]$\simeq +0.2$.

We note, as discussed in Lee et al. 2008, that below 4500 K most of the T_i temperature estimates are from "auxiliary" SSPP $T_{\rm eff}$s. Actually, only by adopting $T3$ we have enough stars to test the validity of our synthetic indices at $T_{\rm eff} < 4000$ K (see Section 3.1.1). Figure 14 shows the "dwarf" stars in the metallicity bin $M_{\rm SSPP}=-0.5$ which is the most populated one. The two right panels show that synthetic isogravities match quite well the observational points also in the region $1.2 < \theta < 1.3$ (i.e., 3875 K $< T_{\rm eff} <$ 4200 K). There is some tendency of the observational points in the left panels to have lower index values than those predicted at very low temperatures. On the other hand, CaHK and Mgb indices depend significantly on log g and we must recall that the selection of points in Figure 14 was performed by using $G_{\rm SSPP}$ and $M_{\rm SSPP}$ which are not self-consistent with $T3$. Even if more accurate determinations of atmospheric parameter values for SDSS stars are required to draw a sound conclusion about the validity of our synthetic library at the coolest temperature, Figure 14 seems to indicate that there are no significant systematic differences between observational and synthetic indices at $T_{\rm eff} < 4000$ K when using $T3$. This fact suggests that the two coolest outliers discussed in Section 3.1.1 and Appendix A.1 may be more likely explained by incorrect parameter values than by intrinsic problems in the coolest part of our Lick/SDSS library.

In the case of "giants" (see Figures 12 and 13) the observed points, independently of the tern of parameters used, always fall to the left (and, sometime, below) of the theoretical lines, indicating that the estimates of $T_{\rm eff}$ for these stars are on a systematically different temperature scale from that one of the

[15] Due to the fact that T, G, and M entries in the table sppParams do not hang together homogeneous terns of parameter estimates have an odd appearance like, for example, ($T6$, $G2$, $M2$) or ($T11$, $G10$, $M12$).

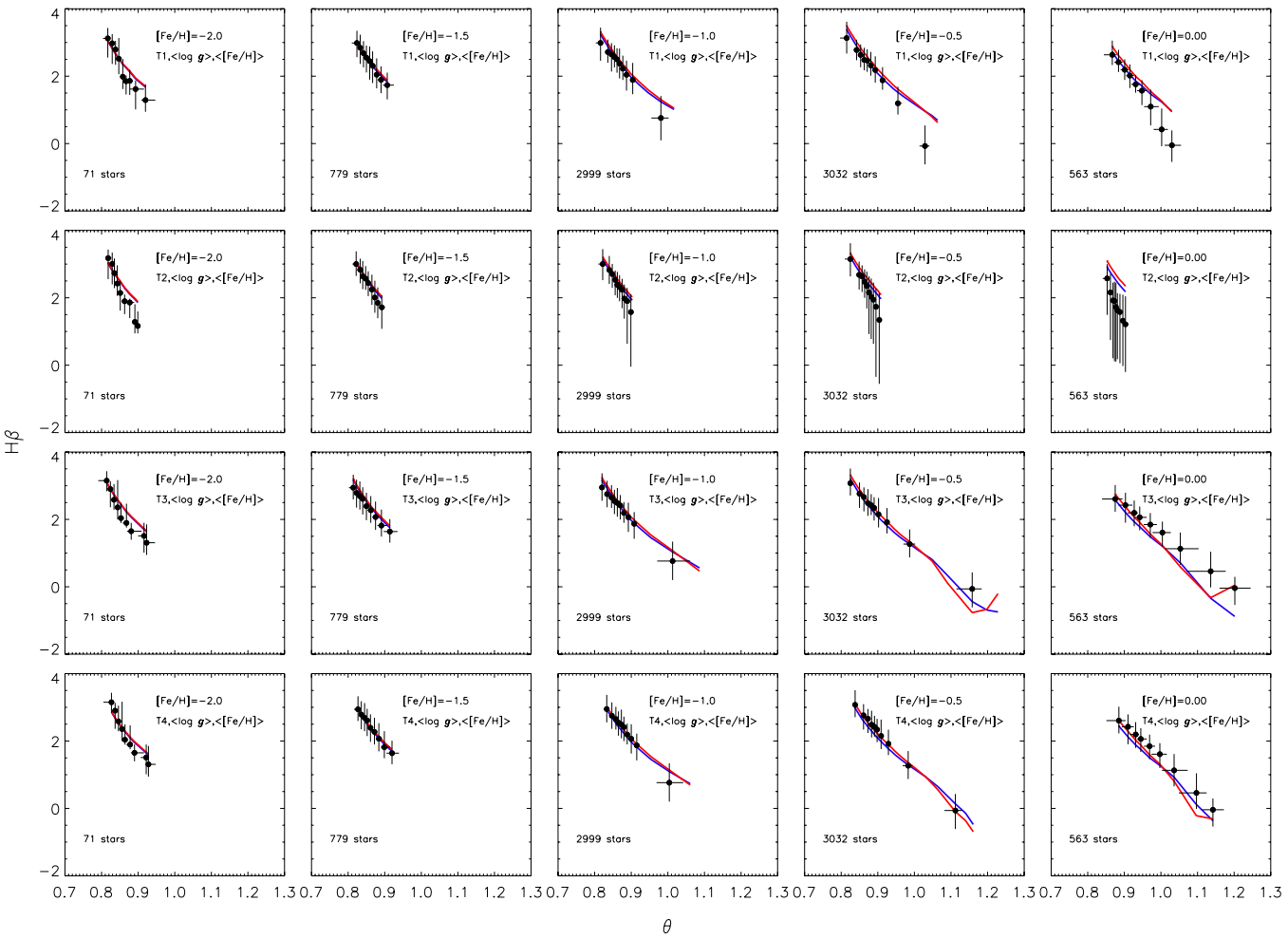

Figure 11. Median values of spectral index Hβ of SDSS–DR7 "dwarf" stars vs. $\theta = 5040/T_{\rm SSPP}$ by using different $T_{\rm eff}$ estimates (rows) in different metallicity groups (columns). Synthetic SSA (blue lines) and NSSA (red lines) are overplotted. Vertical and horizontal bars represent 68% confidence intervals.

(A color version of this figure is available in the online journal.)

EIM sample. It looks like that SSPP temperatures for "giants" are always overestimated with, maybe, the only exception of $T1$ for the highest stellar temperatures and [Fe/H] $=-1.5$. This $T_{\rm eff}$ overestimation very likely introduces also systematic offsets in the log g and [Fe/H] estimates, thus causing errors in assigning individual objects to the surface gravity and metallicity groups and explaining the vertical displacements in some diagrams.

Analysis of Figure 11 indicates that the systematic difference of T_i temperature scales with respect to the EIM one for "dwarfs" have different magnitudes and signs suggesting that a reduction of systematic offsets may be obtained by averaging the different temperature estimates. Therefore, we decided to check if the use of the SSPP average estimates of stellar parameter values in the comparison with Lick/SDSS predictions can, at least partially, overcome the problem of systematic errors. The Figure 15 shows for "dwarfs" the same kind of comparison as in Figure 11 for Hβ, Fe5270, CaHK, and Mgb but adopting the $T_{\rm SSPP}$, $G_{\rm SSPP}$, and $M_{\rm SSPP}$ values even if this tern lack of internal consistency. Actually, the results for Hβ, shown in the first row, indicate that the $T_{\rm SSPP}$ is almost on the same temperature scale of the EIM sample and that our synthetic indices quite well reproduce the behavior of the observational ones as far as the effect of temperature is concerned. This is also true for the metallicity behavior since synthetic Fe5270 values match the observed ones in all the different [Fe/H] bins (see row 2). As far as the [α/Fe] behavior is concerned, some hints may be given by CaHK and Mgb indices which are sensitive mainly to [Ca/Fe] and [Mg/Fe], respectively. As expected, the plots in rows 3 and 4 indicate that the loci of the observational points get closer to the NSSA curves as metallicity decreases. Furthermore, the comparison of the Mgb and CaHK plots indicates, for [Fe/H] $<$ 0.0, a value of [Mg/Fe] higher than that of [Ca/Fe] as already suggested in the literature (e.g., Nissen & Schuster 2009).

The adoption of the average SSPP parameter values for "giants," unfortunately, does not reduce the problem of systematic differences in T_i since, as already mentioned above, all the SSPP effective temperature values, for this class of objects, seem to be overestimated. Therefore, no direct check on the validity of the behavior of Lick/SDSS indices versus surface gravity can be performed by using $T_{\rm SSPP}$, $G_{\rm SSPP}$, and $M_{\rm SSPP}$ for giants.

In conclusion, the use of SDSS data to check the validity of our synthetic indices in reproducing those of real stars is hampered by the uncertainties on the actual values of the stellar $T_{\rm eff}$, log g, and [Fe/H] of SDSS stars. Therefore, it would be very interesting to perform the same kind of analysis on the spectra from the Low Resolution Spectroscopic Survey with LAMOST when available. In fact, the use of a different spectral analysis pipeline for extracting stellar atmospheric parameters (see, for example, Luo et al. 2008) should lead to different (and hopefully smaller) systematic errors.

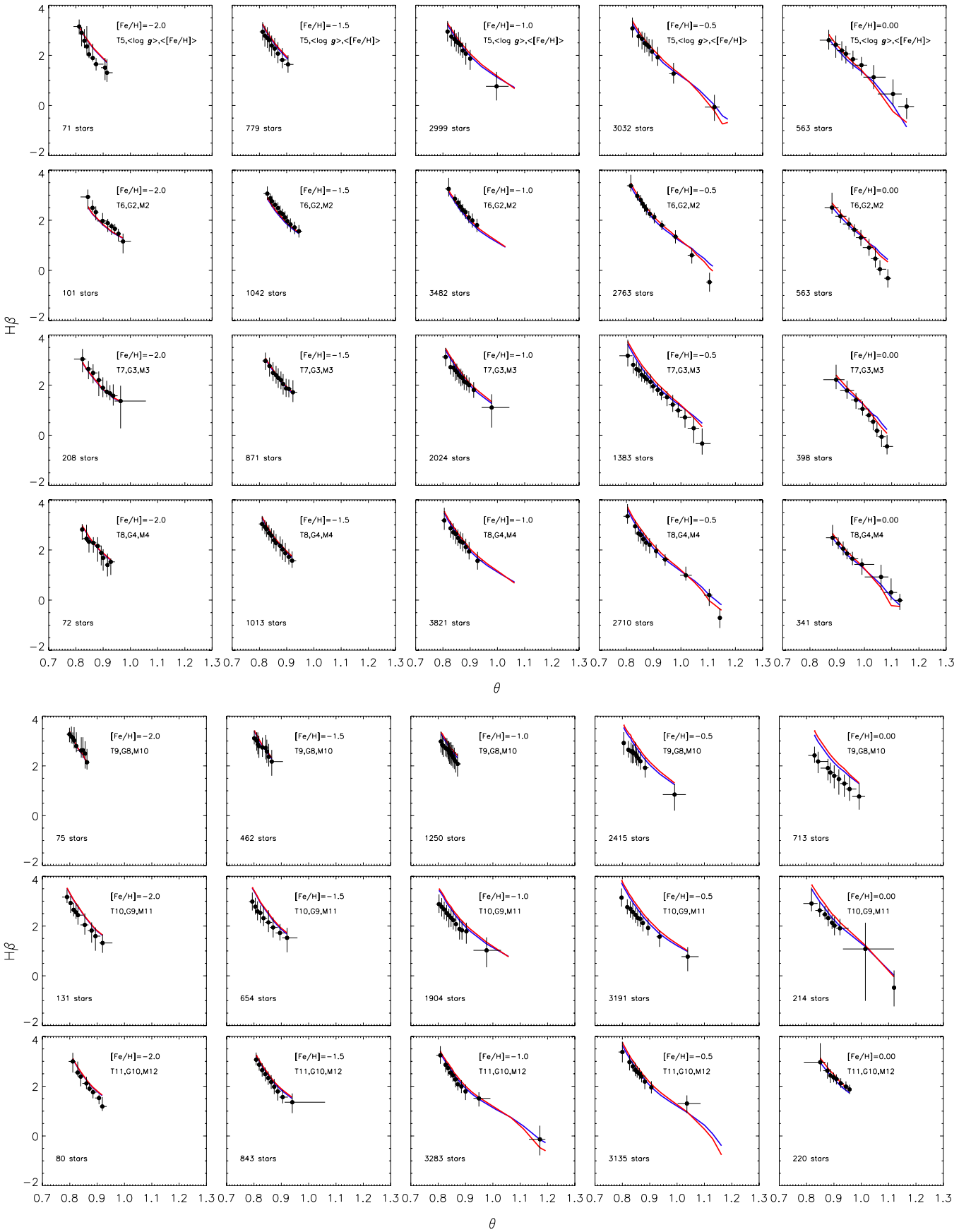

Figure 11. (Continued)

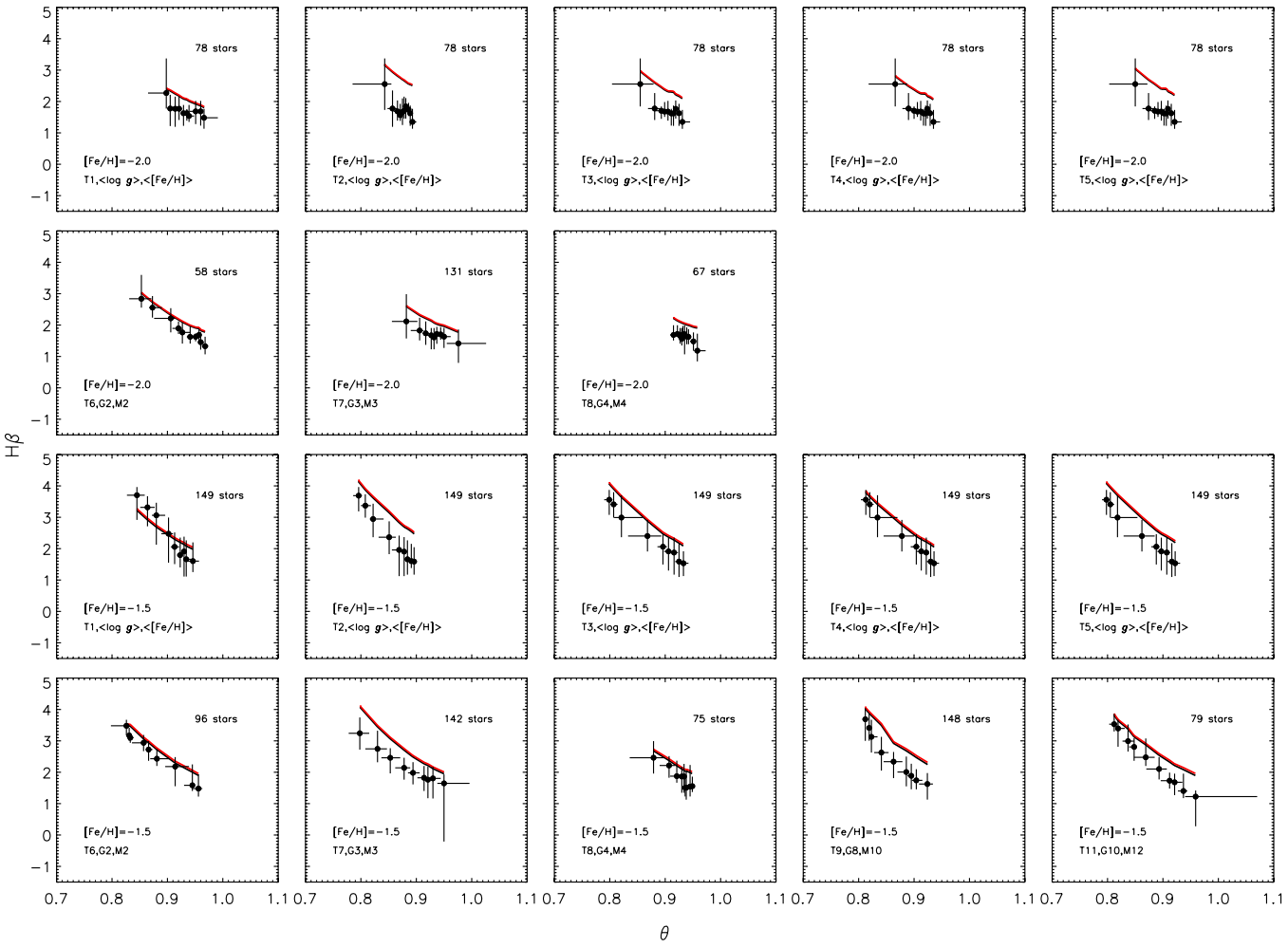

Figure 12. Median values of spectral index Hβ of SDSS–DR7 "giant" stars vs. $\theta = 5040/T_{\rm SSPP}$ by using different $T_{\rm eff}$ estimates for metallicity [Fe/H] $= -2.0$ (first two rows) and [Fe/H] $= -1.5$ (last two rows). Synthetic SSA (blue lines) and NSSA (red lines) are overplotted. Vertical and horizontal bars represent 68% confidence intervals.

(A color version of this figure is available in the online journal.)

5. SUMMARY AND CONCLUSIONS

In this work, we present a synthetic library of spectral feature indices Lick/SDSS ad hoc computed to fully exploit the content of the spectroscopic SDSS–DR7 stellar database which represents the most extended collection of optical data available up to now. The Lick/SDSS system, based on the Lick/IDS one and complemented with an UV index in the wavelength region of Ca II H and K lines, is well suited to study α-element abundances in F, G, and K stars.

The results of the comparison of Lick/SDSS synthetic indices with observational ones can be summarized as follows.

1. The behaviors of Lick/SDSS indices versus effective temperature, surface gravity, metallicity, and α enhancement well reproduce that of observational indices of ELODIE, INDO–U.S., and MILES stars. It is worthwhile to stress that this good agreement is due to the fact that both theoretical and observational indices are on the same temperature scale.
2. The comparison of Lick/SDSS predictions with indices computed from about 17,600 SDSS–DR7 spectra by using single SSPP stellar atmospheric parameter value determinations is significantly affected by systematic differences in the temperature scales.
3. A quite good agreement between Lick/SDSS predictions and observational indices of SDSS–DR7 "dwarf" stars is obtained by using SSPP average estimates of $T_{\rm eff}$, log g, and [Fe/H]. In fact, the average SSPP atmospheric parameter values, even if not self-consistent, reduce the effects of systematic differences among the temperature scales of single SSPP estimates.
4. A significant disagreement is found between Lick/SDSS predictions and the observational indices of SDSS–DR7 "giant" stars. Since this discrepancy is not found for EIM stars, we are confident that the disagreement is a spurious result of systematic overestimates of the SSPP $T_{\rm eff}$ values and not due to flaws in the Lick/SDSS library.

In conclusion, our calibrated library of Lick/SDSS synthetic indices reliably matches the observational picture for F, G, and K stars as checked by using both EIM and SDSS–DR7 objects and, therefore, constitutes a valuable and powerful tool for the study of stellar populations.[16] In particular, its internal accuracy and the fact that it was constructed starting from synthetic spectra at $R = 1800$ makes it well suited to extend the coverage of empirical databases like SDSS and the forthcoming LAMOST

[16] The library of calibrated synthetic indices is available from the authors upon request.

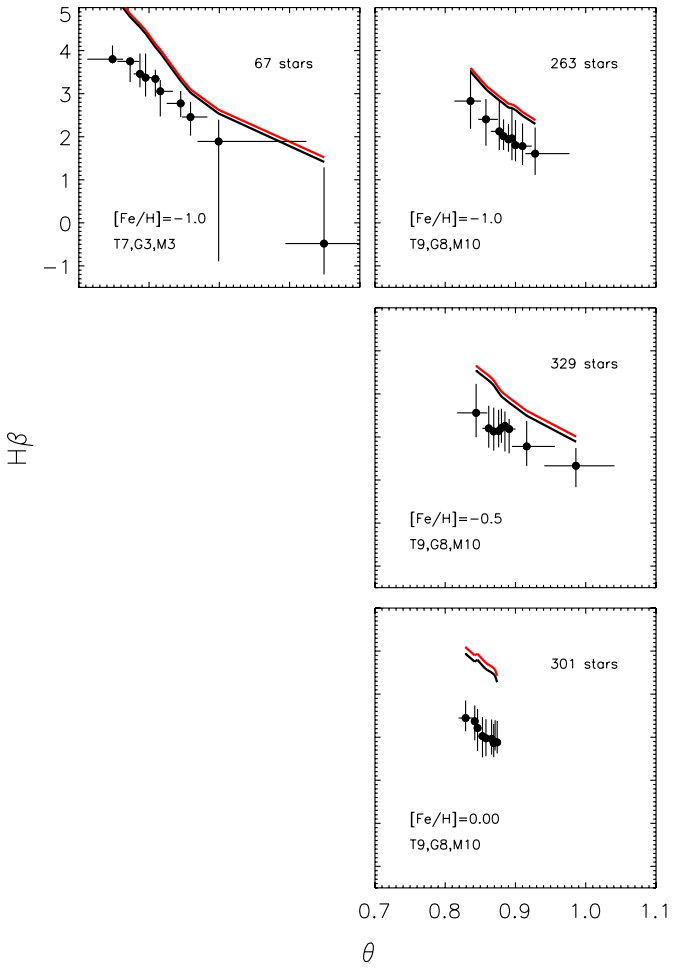

Figure 13. Median values of spectral index Hβ of SDSS–DR7 "giant" stars vs. $\theta = 5040/T_{\rm SSPP}$ for metallicity [Fe/H]> -1.5 by using $T7$ (first column) and $T9$ (second column) estimates. Synthetic SSA (blue lines) and NSSA (red lines) are overplotted. Vertical and horizontal bars represent 68% confidence intervals.
(A color version of this figure is available in the online journal.)

in the parameter space for the analysis of old stellar systems. Moreover, we will use in a forthcoming paper the Lick/SDSS indices to derive estimates of [Ca/Fe] and [Mg/Fe] of individual SDSS–DR7 stars.

We thank the anonymous referee for the constructive report and useful suggestions. This work received partial financial support from the Mexican CONACyT via grant 49231–E, from the Italian MIUR under grant PRIN–INAF 2007 (P. I. Bellazzini).

Funding for the SDSS and SDSS–II has been provided by the Alfred P. Sloan Foundation, the Participating Institutions, the National Science Foundation, the U.S. Department of Energy, the National Aeronautics and Space Administration, the Japanese Monbukagakusho, and the Max Planck Society, and the Higher Education Funding Council for England. The SDSS Web site is http://www.sdss.org/.

The SDSS is managed by the Astrophysical Research Consortium (ARC) for the Participating Institutions. The Participating Institutions are the American Museum of Natural History, Astrophysical Institute Potsdam, University of Basel, University of Cambridge, Case Western Reserve University, The University of Chicago, Drexel University, Fermilab, the Institute for Advanced Study, the Japan Participation Group, The Johns Hopkins University, the Joint Institute for Nuclear Astrophysics, the Kavli Institute for Particle Astrophysics and Cosmology, the Korean Scientist Group, the Chinese Academy of Sciences (LAMOST), Los Alamos National Laboratory, the Max–Planck–Institute for Astronomy (MPIA), the Max–Planck–Institute for Astrophysics (MPA), New Mexico State University, Ohio State University, University of Pittsburgh, University of Portsmouth, Princeton University, the United States Naval Observatory, and the University of Washington.

APPENDIX

OUTLIERS

Table 2 lists the EIM stars classified as outliers (see Sections 3.1.1 and 3.1.2. The stars are divided in two groups, namely, "dwarfs" and "giants," and listed for increasing effective temperatures. The first four columns list the stellar names and the stellar parameter values taken from the original spectral library indicated by the E, I, and M superscripts for ELODIE, INDO–U.S., and MILES, respectively. Column 5 lists the [α/Fe] values as derived from [Mg/Fe] in Borkova & Marsakov (2005). Crosses in Columns 6–24 indicate observational index values which seem to be inconsistent with those predicted from the SSA and/or NSSA grids on the basis of their atmospheric parameters.

In the following sections we discuss individually those stars with more than five entries in Columns 6–24 of Table 2.

A1. "Dwarfs"

Table 2 contains 11 "dwarfs" with more than five entries in the index columns.

1. The first group contains the two stars at the lowest effective temperatures ($T_{\rm eff} < 4000$ K). In both cases, the comparison of the observed spectrum with the synthetic ones from the SSA and NSSA grids at the $T_{\rm eff}$, log g, and [Fe/H] closest to the values given in Table 2 show the presence of weaker observed absorption features than the synthetic ones (see panels *a* and *b* of Figure 16). This fact can be due either to an overestimate of the stellar [Fe/H] values or to an inadequacy of the synthetic spectra at these low temperatures. We discuss this point in Section 4 when we compare our synthetic indices with SDSS observations.
2. There are three stars with $4000 < T_{\rm eff} \leqslant 4500$ and like those in the previous group their observed spectra show weaker absorptions than the synthetic ones. An overestimate of [Fe/H] values for these stars seems more probable than a failure of the synthetic spectra since the index values of other two stars (G19-24 and HD119291) with similar atmospheric parameters are in good agreement with the corresponding synthetic ones.
3. The star HD223524 has a peculiar spectrum since there are regions that are in significant disagreement with the prediction of the synthetic models (see Figure 16(c)). In particular, the stellar calcium and magnesium features seem to indicate a strong under-abundance with respect to iron. A search in the literature provided a high-resolution spectrum (Soubiran et al. 2008) that is in good agreement with the medium-resolution one in MILES thus indicating that the anomalous behavior is not likely to be the result of instrumental artifacts.
4. The comparison of observed and synthetic spectra and the index values of the star BD+15 1305 (see Figure 16(d)) seem to indicate a higher [Fe/H] than the value given in

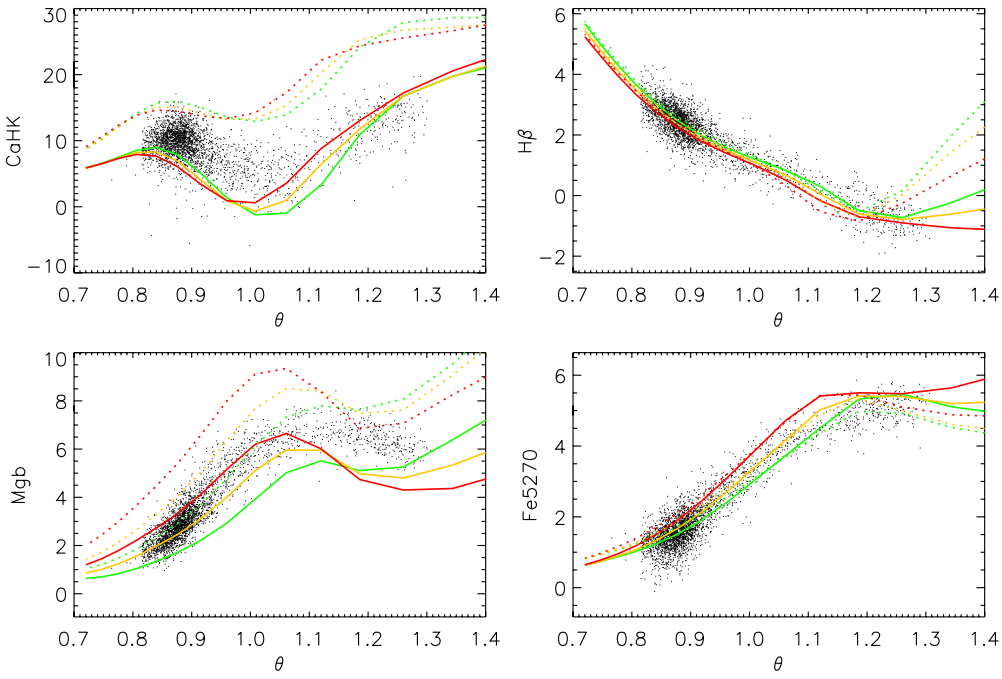

Figure 14. Spectral indices Hβ, Fe5270, CaHK, and Mgb of SDSS–DR7 "dwarf" stars vs. $\theta = 5040/T3$ for $M_{\rm SSPP} = -0.5$. Synthetic SSA (solid lines) and NSSA (dotted lines) isogravities are overplotted: log $g = 4.0$ (green), log $g = 4.5$ (yellow), and log $g = 5.0$ (red).
(A color version of this figure is available in the online journal.)

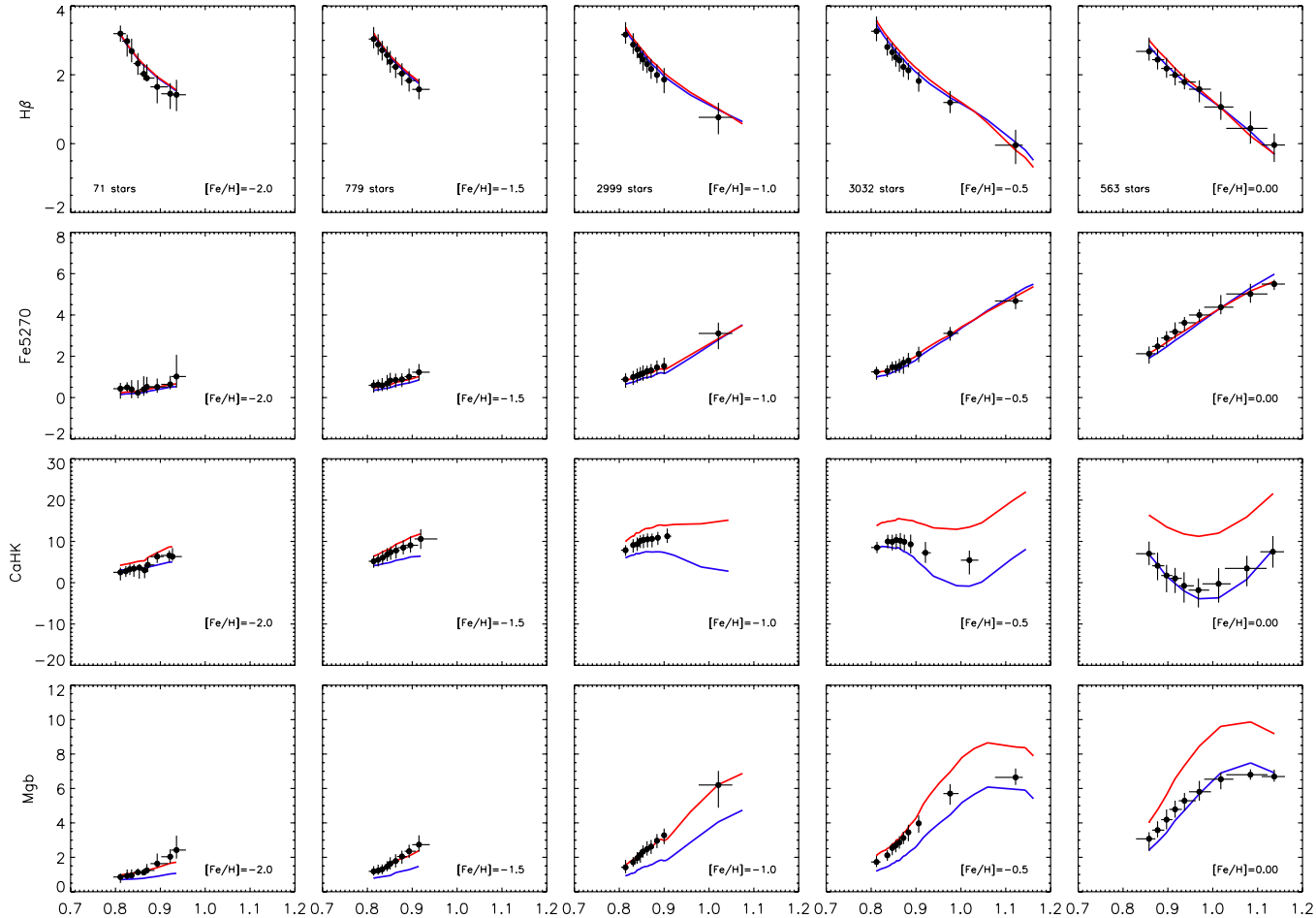

Figure 15. Median values of spectral indices Hβ, Fe5270, CaHK, and Mgb of SDSS–DR7 "dwarf" stars vs. $\theta = 5040/T_{\rm SSPP}$ in different metallicity groups (columns). $G_{\rm SSPP}$ and $M_{\rm SSPP}$ have been used. Synthetic SSA (blue lines) and NSSA (red lines) are overplotted. Vertical and horizontal bars represent 68% confidence intervals.
(A color version of this figure is available in the online journal.)

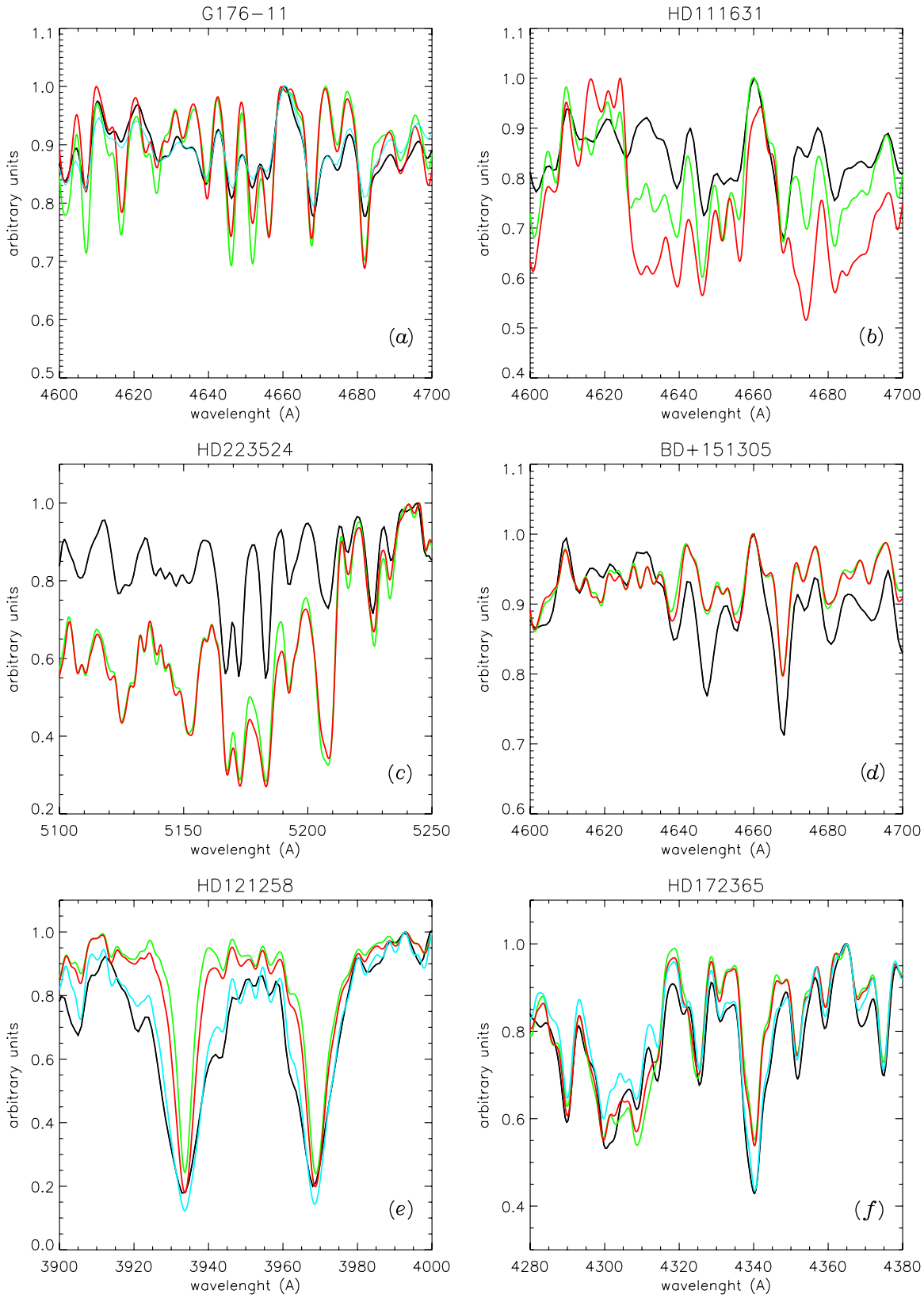

Figure 16. Examples of spectral regions of outlier stars: observed spectrum (black) is overplotted together with SSA (green) and NSSA (red) synthetic ones with atmospheric parameter values from Table 2; light blue lines in (e) and (f) correspond to spectra computed with alternative parameters (see the text).

(A color version of this figure is available in the online journal.)

Table 2. In fact, by assuming [Fe/H] = 0 we get a better agreement in the spectra and we are able to remove this star from the list of outliers.

5. The failure in reproducing the observed index values of G103-68 (G87-12), HD76813, and HD92769 with the synthetic ones is due to wrong parameter values in INDO–U.S.

In fact, the star G82-12 was probably confused with G87-12; HD76813 is actually a giant with $T_{\rm eff} = 5172$, $\log g = 3.08$, and [Fe/H] $= -0.24$ according to Soubiran et al. (2008); and HD92769 has an effective temperature of 8318 K according to Allende Prieto & Lambert (1999).

6. The comparison of observed and synthetic spectra (see Figure 16(e)) and the Hβ index value of the star HD121258 seem to indicate a lower $T_{\rm eff}$ value than 6570 K as given in Table 2 which is highly uncertain since it was derived from the stellar spectral type. Actually, by assuming $T_{\rm eff} = 6250$ we get a better agreement in the spectra.

A2. "Giants"

Table 2 contains three "giants" with more than five entries in the index columns.

1. The observed index values of HD 10486 and its spectrum show stronger features than the synthetic ones. A search in the literature provided a higher surface gravity estimate $\log g = 3.28$ (Allende Prieto & Lambert 1999) instead of 2.80, which could explain, at least partially, the stronger observed indices.
2. The observed index values of HD 12014 and its spectrum indicate a lower effective temperature like that one expected according to the stellar spectral type (i.e., $T_{\rm eff} \sim 4400$ K as in Wright et al. 2003) but this low temperature is inconsistent with the Hβ observed index.
3. The observed index values of HD 172365 and its spectrum indicate a higher effective temperature. A search in the literature provided several alternative set of atmospheric parameter values in a temperature range 5800–6100 K. A quite good agreement between observations and synthetic prediction would be achieved by using $T_{\rm eff} = 6030$, $\log g = 2.22$, and [Fe/H] $= -0.04$ as found by Gray et al. 2001 (see Figure 16(f)).

REFERENCES

Abazajian, K. N., et al. 2009, ApJS, 182, 543
Allende Prieto, C., Beers, T. C., Wilhelm, R., Newberg, H. J., Rockosi, C. M., Yanny, B., & Lee, Y. S. 2006, ApJ, 636, 804 (AP06)
Allende Prieto, C., & Lambert, D. L. 1999, A&A, 352, 555
Borkova, T. V., & Marsakov, V. A. 2005, Astron. Rep., 49, 405
Bruzual, G., & Charlot, S. 2003, MNRAS, 344, 1000
Carollo, D., et al. 2007, Nature, 450, 1020
Castelli, F., & Kurucz, R. L. 2003, in IAU Symp. 210, Modelling of Stellar Atmosphere, ed. N. E. Piskunov, W. W. Weiss, & D. F. Gray (San Francisco, CA: ASP), A20
Cayrel, R., Perrin, M.-N., Buser, R., Barbuy, B., & Coupry, M. F. 1991, A&A, 247, 122
Cenarro, A. J., et al. 2007, MNRAS, 374, 664
Chavez, M., Bertone, E., Buzzoni, A., Franchini, M., Malagnini, M. L., Morossi, C., & Rodriguez-Merino, L. H. 2007, ApJ, 657, 1046
Coelho, P., Barbuy, B., Melendez, J., Schiavon, R. P., & Castilho, B. W. 2005, A&A, 443, 735
Franchini, M., Morossi, C., Di Marcantonio, P., Castelli, F., Malagnini, M. L., & Chavez, M. 2005, ApJ, 634, 1319
Franchini, M., Morossi, C., Di Marcantonio, P., Malagnini, M. L., & Chavez, M. 2004, ApJ, 601, 485
Girard, P., & Soubiran, C. 2005, in Proc. Gaia Symp., The Three-Dimensional Universe with Gaia (ESA SP-576), ed. C. Turon, K. S. O'Flahrty, & M. A. C. Perryman (Noordwijk: ESA), 169
Gray, R. O., & Corbally, D. J. L. I. 1994, AJ, 107, 742
Gray, R. O., Napier, M. G., & Winkler, L. I. 2001, AJ, 121, 2148
Grevesse, N., & Sauval, A. J. 1998, Space Sci. Rev., 85, 161
Jurić, M., et al. 2008, ApJ, 673, 864
Korn, A. J., Maraston, C., & Thomas, D. 2005, A&A, 438, 685
Kurucz, R. L. 1996, in ASP Conf. Ser. 108, Model Atmospheres and Spectrum Synthesis, ed. S. J. Adelman, F. Kupka, & W. W. Weiss (San Francisco, CA: ASP), 2
Le Borgne, D., Rocca-Volmerange, B., Prugniel, P., Lançon, A., Fioc, M., & Soubiran, C. 2004, A&A, 425, 881
Lee, H. C., et al. 2009, ApJ, 694, 902
Lee, Y. S., et al. 2008, AJ, 136, 2022
Luo, A., Wu, Y., Zhao, J., & Zhao, G. 2008, Proc. SPIE, 7019, 701935-1
Maraston, C. 2005, MNRAS, 362, 799
Moultaka, J., Ilovaisky, S. A., Prugniel, P., & Soubiran, C. 2004, PASP, 116, 693
Newberg, H. J., et al. 2009, Bull. Am. Astron. Soc., 41, 229
Nissen, P. E., & Schuster, W. J. 2009, in IAU Symp. 254, The Galactic Disk in Cosmological Context, ed. J. Andersen, J. Bland-Hawthorn, & B. Nordström (Cambridge: Cambridge Univ. Press), 103
Re Fiorentin, P., Bailer-Jones, C. A. L., Lee, Y. S., Beers, T. C., Sivarani, T., Wilhelm, R., Allende Prieto, C., & Norris, J. E. 2007, A&A, 467, 1373
Schiavon, R. P. 2007, ApJS, 171, 146
Serven, J., Wortey, G., & Briley, M. M. 2005, AJ, 627, 754
Soubiran, C., Bienayme, O., Mishenina, T. V., & Kovtyukh, V. V. 2008, A&A, 480, 91
Trager, S. C., Faber, S. M., & Dressler, A. 2008, MNRAS, 386, 715
Tripicco, M. J., & Bell, R. A. 1995, AJ, 110, 3035
Valdes, F., Gupta, R., Rose, J. A., Singh, H. P., & Bell, D. J. 2004, ApJS, 152, 251 (INDO–U.S.)
Valenti, J. A., & Fischer, D. A. 2005, ApJS, 159, 141 (SPOCS)
Vazdekis, A. 1999, ApJ, 513, 224
Willemsen, P. G., Hilker, M., Kayser, A., & Bailer-Jones, C. A. L. 2005, A&A, 436, 379
Worthey, G., Faber, S. M., Gonzalez, J. J., & Burstein, D. 1994, ApJS, 94, 687 (WFGB94)
Worthey, G., & Ottaviani, D. L. 1997, ApJS, 111, 377
Wright, C. O., Egan, M. P., Kraemer, K. E., & Price, S. D. 2003, AJ, 125, 359
York, D. G., et al. 2000, AJ, 120, 1579
Zhao, G., Chen, Y., Shi, J., Liang, Y., Hou, J., Chen, L., Zhang, H., & Li, A. 2006, Chin. J. Astron. Astrophys., 6, 265